Repurposing of mitochondria-targeted tamoxifen: Novel anti-cancer drug exhibits potent activity against major protozoan and fungal pathogens.

Dominik Arbon[1*], Kateřina Ženíšková[1*], Karolína Šubrtová[1], Jan Mach[1], Jan Štursa[2], Marta Machado[4], Farnaz Zahedifard[1], Tereza Leštinová[5], Carolina Hierro-Yap[6], Jiri Neuzil[2,7,8], Petr Volf[5], Markus Ganter[3], Martin Zoltner[1], Alena Zíková[6,9#], Lukáš Werner[2#], Robert Sutak[1#]

[1] Department of Parasitology, Faculty of Science, Charles University, BIOCEV, Vestec, Czech Republic

[2] Institute of Biotechnology, Czech Academy of Sciences, Vestec, Prague-West, Czech Republic

[3] Centre for Infectious Diseases, Parasitology, Heidelberg University Hospital, Im Neuenheimer Feld 344, 69120, Heidelberg, Germany

[4] Graduate Program in Areas of Basic and Applied Biology, Instituto de Ciências Biomédicas Abel Salazar, Universidade do Porto, Portugal

[5] Faculty of Sciences, Charles University, Department of Parasitology, Prague, Czech Republic

[6] Institute of Parasitology, Biology Centre, Czech Academy of Sciences, Branišovská 31, 37005, České Budějovice, Czech Republic

[7]School of Pharmacy and Medical Science, Griffith University, Parklands Avenue, Southport 4222, Qld, Australia

[8]Depatment of Physiology, Faculty of Science, Charles University, Prague 2, Czech Republic

[9] Faculty of Science, University of South Bohemia, Branišovská 31, 37005, České Budějovice, Czech Republic

[*] These authors have equal contribution

[#] Corresponding authors: sutak@natur.cuni.cz, Lukas.Werner@ibt.cas.cz, azikova@paru.cas.cz

Abstract

Many of the currently available anti-parasitic and anti-fungal frontline drugs have severe limitations, including adverse side effects, complex administration, and increasing occurrence of resistance. The discovery and development of new therapeutic agents is a costly and lengthy process. Therefore, repurposing drugs with already established clinical application offers an attractive, fast-track approach for novel treatment options. In this study, we show that the anti-cancer drug MitoTam, a mitochondria-targeted analog of tamoxifen, efficiently eliminates a wide range of evolutionarily distinct pathogens *in vitro*, including pathogenic fungi, *Plasmodium falciparum*, and several species of trypanosomatid parasites, causative agents of debilitating neglected tropical diseases. MitoTam treatment was also effective *in vivo* and significantly reduced parasitemia of two medically important parasites, *Leishmania mexicana* and *Trypanosoma brucei*, in their respective animal infection models. Functional analysis in the bloodstream form of *T. brucei* showed that MitoTam rapidly altered mitochondrial functions, particularly affecting cellular respiration, lowering ATP levels, and dissipating mitochondrial membrane potential. Our data suggest that the mode of action of MitoTam involves disruption of the inner mitochondrial membrane, leading to rapid organelle depolarization and cell death. Altogether, MitoTam is an excellent candidate drug against several important pathogens, for which there are no efficient therapies and for which drug development is not a priority.

Author Summary

MitoTam, a mitochondrially targeted analog of tamoxifen, is a promising anti-cancer candidate drug acting by accumulating in and destabilizing cell mitochondria. In this study, we analyze its effect on a wide range of evolutionarily distinct and medically important pathogens. These include a) pathogenic fungi, *Candida albicans,* and *Cryptococcus neoformans,* ubiquitous opportunistic pathogens that cause life-threatening diseases in immunocompromised or immunologically deficient individuals; b) *Plasmodium falciparum*, the causative agent of human malaria; and c) several species of trypanosomatid parasites such as *Trypanosoma cruzi,* responsible for deadly Chagas disease in South America, *Trypanosoma brucei,* the causative agent of sleeping sickness in Africa, and *Leishmania, the* etiological agent of leishmaniasis, a spectrum of diseases ranging from usually self-healing but potentially disfiguring cutaneous and mucocutaneous leishmaniasis, to visceral leishmaniasis, which is invariably fatal if left untreated. We show that MitoTam efficiently kills these parasites in laboratory conditions and in the case of trypanosomes and leishmaniases suppress or at least slow down the infection in mouse model.

Introduction

The ongoing search for novel treatment options to combat medically relevant parasitic protists (e.g. *Plasmodium*, *Trypanosoma* and *Leishmania spp.*) is driven by the need for more efficient, less toxic, and/or less expensive medications as well as by the emergence and spread of drug resistance [1–3]. Drug discovery and development have been facilitated in recent decades by advances in the fields of genetics, molecular biology, medicinal chemistry and the introduction of high throughput target-based, phenotypic and virtual screening strategies. Nevertheless, repurposing of drugs originally approved for other indications presents a strategy of particular interest for the implementation of novel treatments for neglected diseases [3]. As repurposed drugs are typically at least partly characterized or even approved for clinical use, both the time and cost of the drug development process are dramatically reduced. This is particularly appealing for drugs against neglected diseases with little financial incentive for commercial '*de novo*' drug discovery approaches.

Phosphonium salts are lipophilic cations with the ability to readily pass across phospholipid bilayers, and due to their delocalized positive charge, they accumulate at the interface of the inner mitochondrial membrane (IMM) and matrix according to the mitochondrial membrane potential ($\Delta\Psi_m$). The extent of accumulation of lipophilic cations at the IMM follows the Nernst equation, according to which there is a tenfold increase in the concentration of lipophilic cations at the IMM-matrix interface for every ~60 mV increase in $\Delta\Psi_m$ [4]. Phosphonium vectors have been employed for efficient and selective mitochondrial delivery of various cargo molecules such as therapeutic antioxidants [5,6], liposomes [7], functional probes [8,9], anti-microbial, anti-fungal and anti-parasitic drugs [10–16] and anti-cancer treatments [10,17,18].

MitoTam, mitochondrially targeted cationic triphenylphosphonium vector (TPP^+) conjugated with tamoxifen, is a promising anti-cancer candidate drug acting by mitochondrial destabilization [19]. It was originally developed to selectively accumulate the pharmacophore tamoxifen in the mitochondria proportionally to $\Delta\Psi_m$. The compound is well tolerated in the mouse model and recently underwent

a phase 1/1b clinical trial in human advanced-stage cancer patients with favorable outcome (MitoTam-01 trial; EudraCT 2017-004441-25). Its molecule consists of three parts: i) the functional pharmacophore residue, tamoxifen, a drug that has been used for decades to treat early and advanced hormone-dependent breast cancer [20], ii) the TPP^+ for mitochondrial targeting, and iii) the ten-carbon linear alkyl linker tethering tamoxifen to the TPP^+ moiety. The compound efficiently kills breast cancer cells and suppresses tumors progression, including treatment-resistant carcinomas with high Her2 protein levels ($Her2^{high}$), for which the original precursor compound tamoxifen was ineffective. Importantly, MitoTam exhibits low toxicity towards non-malignant cells [19]. Similar to the mitochondria-mediated anti-cancer effects of tamoxifen, MitoTam modulates or alters multiple mitochondrial processes including the function of the respiratory complex I (CI; NADH:ubiquinone dehydrogenase) [19,21–23]. The superior efficacy of MitoTam compared to tamoxifen is due to its accumulation at the interface of the mitochondrial matrix and IMM that leads to suppression of CI-dependent respiration, disruption of respiratory supercomplexes, rapid dissipation of the $\Delta\Psi_m$, increased production of reactive oxygen species (ROS), and ultimately cell death [19]. MitoTam is also effective in the treatment of the syngenic renal cancer murine model, especially in combination with immunotherapy [23]. In addition, MitoTam selectively eliminates senescent cells and is, therefore, a candidate for the treatment of age-related disorders [22,24].

In this work, we tested the potential activity of MitoTam against a wide range of parasitic protists and pathogenic fungi (Table S1). These models were selected for their medicinal and economic relevance and for their suitability as cellular models for research of mitochondrial function. We chose parasites from the Kinetoplastida group: *Trypanosoma brucei* as a causative agent of human and animal African trypanosomiases and a highly tractable model organism; *Trypanosoma cruzi*, an intracellular parasite responsible for Chagas disease; and *Leishmania spp.*, the etiological agent of a spectrum of disorders ranging from self-healing cutaneous lesions to potentially fatal visceral diseases [25]. We also tested the effect of MitoTam on *Plasmodium falciparum*, a parasite responsible for most malaria-related deaths in humans [26]; on the pathogenic fungi *Candida albicans* and *Cryptococcus neoformans*,

widespread opportunistic pathogens causing life-threatening diseases in immunocompromised individuals [27,28]; on the amphizoic amoebae *Naegleria fowleri* and *Acanthamoeba* spp., whose infections lead to rare diseases with extremely high mortality rate [29,30]; and on *Giardia intestinalis* and *Trichomonas vaginalis*, anaerobic parasites with reduced mitochondria, causative agents for widespread intestinal and urogenital infections [31–33]. Here, we show that the anti-cancer drug candidate MitoTam efficiently and selectively inhibits viability of a number of these pathogens *in vitro*. In pilot experiments using mouse models of infection with *T. brucei* and *L. mexicana*, MitoTam reduced parasite burdens and significantly prolonged survival for *T. brucei*-infected animals. Furthermore, we demonstrate in *T. brucei* that the trypanocidal activity of MitoTam relies, at least partly, on rapid disruption of IMM. Together, our data provide strong evidence that MitoTam is an excellent candidate for further development as an anti-infective, especially for targeting several neglected diseases.

Results

Low levels of MitoTam are lethal to a variety of pathogenic eukaryotic microorganisms.

The mitochondrion is a promising drug target because of its pivotal role in cellular metabolism, proliferation, and cell death signaling [34–36]. We therefore investigated the effect of MitoTam, a mitochondria-targeted tamoxifen derivative, on a wide range of parasitic protists and yeasts. MitoTam proved to have a significant growth inhibitory effect for the majority of these pathogens (Table 1) exhibiting nanomolar potencies against *P. falciparum*, *T. b. brucei* and *Leishmania spp.* Notably, the half-maximal effective concentration (EC_{50}) values are considerably lower than corresponding cytotoxicity values reported for various mammalian cells (ranging from 0.65-4.5 µM) [19], indicating high selectivity. All pathogens were also challenged with the parental compound tamoxifen lacking the TPP^+ vector for mitochondrial targeting, with efficacy significantly lower compared to MitoTam (Table 1). This is consistent with similar comparisons reported for the anti-cancer activity of the two

130 molecules [19]. Each dose-response analysis was validated using a known, active compound against
131 individual pathogens tested, providing values consistent with published data (Table 1).

Pathogen	MitoTam		Tamoxifen		Control compound		
	EC_{50} [µM]	SD	EC_{50} [µM]	SD		EC_{50} [µM]	SD
Trypanosoma brucei BSF	0,02	±0.00	7,20	±1.47	amphotericin B	1,09	±0.09
Trypanosoma brucei PCF	0,16	±0.03	≥ 10		amphotericin B	0,24	±0.06
T.brucei gambiense BSF	0,03	±0.00	≥ 10		pentamidine	0,00	±0.00
Trypanosoma cruzi (epimastigotes)	1,55	±0.04	≥ 10		benznidazole	≥ 10	
Leishmania mexicana (amastigotes)	0,35	±0.05	7,93	±0.59	amphotericin B	0,33	±0.08
Leishmania major (promastigotes)	0,60	±0.10	≥ 10		amphotericin B	0,06	±0.02
Plasmodium falciparum (erythrocytic stage)	0,03	±0.01	6,37	±0.11	chloroquine	0,01	±0.00
Candida albicans	0,56	±0.07	≥ 10		amphotericin B	0,37	±0.01
Cryptococcus neoformans	0,61	±0.12	7,28	±1.97	amphotericin B	0,12	±0.05
Naegleria fowleri	≥ 10		≥ 10		amphotericin B	0,08	±0.01
Acanthamoeba spp.	1,95	±0.23	9,93	±0.58	amphotericin B	6,17	±0.70
Giardia intestinalis	≥ 10		≥ 10		benznidazole	6,22	±0.66
Trichomonas vaginalis	≥ 10		≥ 10		metronidazole	6,54	±0.45

132 **Table 1: MitoTam inhibits the growth of several pathogenic microorganisms *in vitro*.** Mean EC_{50}
133 values for MitoTam, tamoxifen (the functional pharmacophore of MitoTam) and specific anti-
134 microbial drugs used as positive controls for each tested organism derived from dose-response curves
135 are given in µM (n>3, ± s.d.).
136

137 The highest efficacy of MitoTam was detected for the bloodstream form (BSF) of *T. brucei*. This value
138 was approximately 30-fold greater compared to $Her2^{high}$ cancer cells (0.02 µM *vs* 0.65 µM) [19].
139 Interestingly, MitoTam showed low nanomolar efficacy (0.03 µM) against the erythrocytic stage of *P.*
140 *falciparum*, which is protected inside the parasitophorous vacuole within the host erythrocyte [37],
141 suggesting that MitoTam is able to cross several membranes before reaching its target. Furthermore,
142 MitoTam was found to inhibit the growth of the *T. brucei* procyclic form (PCF), axenically grown
143 *Leishmania mexicana* amastigotes and *L. major* promastigotes, and the two pathogenic fungi *Candida*
144 *albicans* and *Cryptococcus neoformans* at sub-micromolar EC_{50} values. *T. cruzi* epimastigotes also
145 responded to MitoTam treatment with low-micromolar EC_{50}, as did *Acanthamoeba spp.*, while no

146 effect was observed on *Naegleria fowleri* proliferation. Also, *Trichomonas vaginalis* and *Giardia*
147 *intestinalis*, two anaerobic parasites that possess mitochondrion-related organelles characterized by
148 the absence of membrane-bound electron transport chain and therefore by the lack of mitochondrial
149 respiration [33], were insensitive to MitoTam treatment. Overall, MitoTam effectively eliminated a
150 range of clinically important, evolutionarily distinct pathogens including intracellular parasites.

151

152 **MitoTam efficiently eliminates *L. major* and *L. infantum* intracellular amastigotes.**

153 The high efficacy of MitoTam against *L. mexicana* axenic amastigotes (EC_{50} 0.35 ± 0.05 μM) prompted
154 us to investigate the ability of MitoTam to eliminate the intracellular form of the parasite in a
155 macrophage infection model. Murine macrophage cells (J774A.1) were infected with *L. major* or *L.*
156 *infantum* promastigotes and exposed to different concentrations of MitoTam (0-25μM). After
157 controlled lysis of the infected macrophages, the released parasites were quantified using a resazurin-
158 based viability assay [38]. In this intramacrophage assay, treatment with MitoTam eliminated
159 intracellular amastigotes of *L. major* and *L. infantum* with EC_{50} values of 175 ± 51 nM and 293 ± 29 nM,
160 respectively (Fig. S1). This result is highly encouraging since the parasites reside in a parasitophorous
161 vacuole, a phagolysosome-like structure with low pH and three membranes that make it difficult to
162 effectively target the intracellular *Leishmania* amastigotes *in vivo* [38].

163

164 **MitoTam treatment alleviates parasitemia leading to prolonged survival of mice infected with *T.***
165 ***brucei* and to reduced frequency and lesion size caused by *L. mexicana* infection.**

166 Activity for a compound series detected in the intramacrophage assay usually translates into activity
167 in an animal infection model [39,40], apart from potential issues with pharmacokinetics. Hence, we
168 next tested the ability of MitoTam, which is well tolerated in BALB/c mice [19], a mouse infection
169 model of both *L. mexicana* and *T. brucei.* MitoTam dosing regimen was based on the published data
170 [19,22].

For the *T. brucei* infection model, survival analysis revealed that MitoTam intravenous (IV) administration at doses of 3 mg/kg body weight (bw) on days 3 and 5 post-infection without further treatment delayed the death of *T. brucei* infected animals, which succumb to the infection by eight days (Fig. 1A).

In a second experiment, we followed *T. brucei* parasitemia levels in infected animals (Fig. 1B). Automated analysis of blood smears revealed the presence of *T. brucei* parasites in samples from mice untreated and treated on days 2 and 4 post-infection, showing that MitoTam-treated animals exhibited a significantly lower parasite load (Fig. 1B). This explains the longer survival of treated animals compared to the untreated controls (Fig. S2).

The effect of MitoTam administration (3 mg/kg bw, intraperitoneally (IP)) in the *L. mexicana* infection model was assessed by monitoring frequency and size of dermal lesions. As shown in Fig. 1C, lesions occurred less frequently in MitoTam-treated BALB/c mice than in the untreated controls during the 12-week course of the experiment (50% vs. 90% of mice at weeks 8-12 post-infection). In a separate experiment, MitoTam at two doses reduced the size of lesions caused by *L. mexicana* in the weeks following infection (Fig. 1D).

Collectively, these data demonstrate that MitoTam is highly effective against *T. brucei* and *L. mexicana* parasites *in vivo*. Notably, we did not observe any notable adverse effects of MitoTam on the treated animals.

MitoTam treatment causes alteration of *T. brucei* mitochondrial proteome and leads to upregulation of multidrug efflux pumps in *C. albicans*.

The potent anti-parasitic properties *in vitro* and the promising *in vivo* experiments prompted us to explore the MitoTam mode of action. First, we performed comparative whole-cell proteomic analysis of control and MitoTam-treated cells for two parasitic model organisms, *C. albicans* and *T. brucei.* In

order to restrict indirect, secondary impact resulting from cell death, we chose short exposure times: yeast cells were treated with 4.4 µM MitoTam (□7x EC_{50}) for 12 h, while *T. brucei* BSF cells were incubated with 100 nM MitoTam (5x EC_{50}) for 14 h. Proteomic data were processed by label-free quantification in MaxQuant [41] and statistically analyzed in Perseus [42,43]. In *C. albicans*, out of 1,950 detected protein groups, the abundance of only 1.69% of the quantified proteins was significantly altered (Table S2) (Fig. 2A), with two homologs of multidrug efflux pumps being among the most upregulated genes (≥26 times).

In contrast, analysis of the *T. brucei* proteome revealed substantial changes after treatment with MitoTam, with 26.3% of all identified proteins (2,063) significantly altered (Table S3) (Fig. 2B). Data analyses did not reveal any specific single pathway or protein as a direct target of MitoTam. Since MitoTam specifically affects mitochondrial functions in various cells [19,22,23], we analyzed enrichment of mitochondrial proteins using a *T. brucei* mitoproteome database [44]. While mitochondrial proteins accounted for 14.3% of all detected proteins, we observed an almost 2-fold enrichment (27.6%) in the significantly altered subset of proteins, with 20.8% and 32.1% in the increased and decreased cohort, respectively. These results indicate that MitoTam treatment induces preferentially a decrease in the levels of various mitochondrial proteins. To validate these results, we analyzed *T. brucei* whole cell lysates from cultures harvested at 4 different time points of MitoTam exposure (8, 12, 16, and 24 h) by immunoblotting with antibodies against 8 mitochondrial marker proteins and cytosolic pyruvate kinase as a control (Fig. 2C). Consistent with the *T. brucei* proteomics analysis, we detected significant abundance decrease for seven mitochondrial proteins after 8 h of MitoTam treatment.

MitoTam treatment leads to disruption of the mitochondrial inner membrane and rapid loss of $\Delta\Psi_m$ in the bloodstream form of *T. brucei*.

MitoTam was reported to directly impact mitochondrial function in renal and breast cancer cells, tumors, and senescent cells [19,22,23]. In line with this, our proteomic analysis indicated that MitoTam treatment perturbs the mitochondrial proteome in *T. brucei*. *T. brucei* BSF cells lack cytochrome-mediated mitochondrial electron transport chain, respiring exclusively via an alternative pathway consisting of mitochondrial glycerol-3-phosphate dehydrogenase and trypanosome alternative oxidase (AOX), and sustaining the $\Delta\Psi_m$ by reversed activity of F_oF_1-ATP synthase [45–47]. Importantly, the cancer molecular target of MitoTam, respiratory CI [19] was shown to be dispensable for BSF cells [48], yet our data show that the drug efficiently eliminates these parasites.

To gain deeper insight into the anti-parasitic mode of action of MitoTam, we investigated its effect on mitochondria in this model protist. When comparing the growth of untreated cells with cells treated with two different concentrations of MitoTam, we found that growth of *T. brucei* cells was significantly inhibited after 24 h (40 nM, 2x EC_{50}) or 12 h (100 nM, 5x EC_{50}) (Fig. 3A). To establish a timeline for further experiments, we performed a live/dead cell assay using the cell-impermeant dye Sytox. This result shows that despite the reduced growth rate, 82.4 % and 71% cells were still viable upon 40 nM and 100 nM MitoTam treatment, respectively, after exposure to the drug for 16 h. At 24 hours of treatment, the viability was further decreased to 67.3% and 63.6% at 40 and 100 nM MitoTam, respectively (Fig. 3B)). This was accompanied by increased level of cellular ROS of cells treated with 100 nM MitoTam for 16 h (Fig. 4A).

To examine whether MitoTam affects mitochondrial activity, we analyzed changes in several cellular attributes associated with mitochondrial function. *T. brucei* BSF cultures were treated for 16 and/or 24 h with 40 nM or 100 nM of MitoTam. We found that incubation with 100 nM MitoTam significantly reduced glycerol-3-phosphate-dependent respiration, increased cellular ADP/ATP ratio (by 2.6-fold), and decreased mitochondrial and cytosolic ATP as well as total cellular ATP levels (Fig. 4B-E). Next, we

assessed $\Delta\Psi_m$ in live cells using the cell-permeable red fluorescent dye TMRE and using the Safranin O assay in digitonin-permeabilized cells. The results of both assays demonstrate that treatment with 100 nM MitoTam rendered the cell incapable of maintaining $\Delta\Psi_m$ (Fig. 4F,G). Moreover, using mitochondrial superoxide indicator (MitoSOX), we detected a significant decrease of mitochondrial ROS levels upon MitoTam treatment, suggesting that the mode of action of MitoTam in trypanosomes differs from its effect in cancer cells (Fig. 4J). Experiments with cultures treated with MitoTam at 40 nM showed a similar but less pronounced overall effect on *T. brucei* mitochondrial activity (Fig. S3).

In agreement with these results, fluorescent microscopy evaluation revealed that treatment with 1 µM MitoTam for 1 h led to an □8-fold decrease of the signal intensity of MitoTracker Red CMX-ROS, a mitochondrial probe used to stain live cells that relies on $\Delta\Psi_m$ (Fig. 4H).

Furthermore, $\Delta\Psi_m$ was assessed in digitonin-permeabilized wild-type BSF cells by Safranine O dye upon addition of ATP. We found that $\Delta\Psi_m$ was quickly dissipated with 1 µM MitoTam, a phenotype dentical to the effect of addition of oligomycin, an inhibitor of ATP synthase (Fig. 4I). Moreover, using mitochondrial superoxide indicator (MitoSOX), we detected a significant decrease of mitochondrial ROS levels upon MitoTam treatment, suggesting that the mode of action of MitoTam in trypanosomes differs from its effect in cancer cells (Fig. 4J).

While the observed changes in the evaluated attributes are consistent with inhibition of FoF1-ATP synthase that generates $\Delta\Psi_m$ in BSF *T. brucei* cells [46], we also tested if the rapid drop in $\Delta\Psi_m$ is caused by non-specific disruption of the IMM. To this end, we assessed the integrity of isolated mitochondria using the mitochondrial marker threonine dehydrogenase (TDH), whose activity is detectable only if the added substrate threonine can freely pass through 'compromised' mitochondrial membrane. As shown in Fig. 4K, treatment with MitoTam at 7.4 µM decreased mitochondrial membrane integrity by 50%. This relatively high value (369 times higher than EC_{50}) determined in this *in vitro* experiment can be explained by a need to form much larger membrane pores for threonine (molecular weight 119.12 g/mol) to enter mitochondria when compared to the formation of much

smaller or temporal pores allowing the passage of H^+. In addition, in this experiment, the BSF form mitochondria is not energized due to the lack of substrates and therefore this could have prevented accumulation of MitoTam from in the organelle. Taken together, these data indicate that MitoTam rapidly disrupts the integrity of the IMM, which leads to the $\Delta\Psi_m$ collapse and cell death.

Discussion

In cancer cells, MitoTam was shown to inhibit CI-dependent respiration, which leads to a rapid decrease of $\Delta\Psi_m$, increased ROS production, and disruption of respiratory supercomplexes. These effects ultimately trigger cell death. The phenotype is even more pronounced in cancer cells, which exhibit high levels of the Her2 protein in mitochondria and elevated CI-dependent respiration. Consistently, mammalian cells deficient in CI are more resistant to MitoTam [19]. In metabolically active senescent cells, MitoTam treatment led to increased levels of ROS, reduced ΔΨm, impaired mitochondrial morphology, and metabolic switching to glycolysis for cellular ATP generation [22]. Interestingly, the mitochondrial phenotype was alleviated and cell survival prolonged in MitoTam-treated senescent cells overexpressing adenine nucleotide translocase-2 (ANT2), which imports ATP into mitochondria [22]. Furthermore, restriction of glycolytic pathways, either by limiting substrate levels or by adding glycolytic inhibitors competing with glucose sensitized control cells to MitoTam [22]. In contrast to cancer cells, ROS scavengers failed to rescue MitoTam-treated senescent cells from death. Moreover, treatment with established CI inhibitors (rotenone and piericidin A) alone did not selectively eliminate senescent cells, while they are sensitive to MitoTam treatment [22]. Therefore, the senolytic effect of MitoTam appears to involve additional mechanisms to CI inhibition. Taken together, the effect of MitoTam on cancer and senescent cells seems to be complex and includes targeting of CI, mitochondrial membrane depolarization, loss of ATP, increased levels of ROS, and possibly interplay between ATP/ADP exchange mechanism and ATP synthase [19,22].

In this study, we showed that MitoTam inhibits the growth of a variety of parasitic protists and fungi. Different sensitivity to the compound may reflect different metabolic adaptations that the pathogens have developed to thrive in their host organism. High potencies were determined for *T. brucei* BSF and for the erythrocytic stage of *P. falciparum*, the relevant life cycle stages persisting in the mammalian host of both these medically important parasites. Notably, canonical CI is missing in *P. falciparum* [49] and is dispensable in BSF *T. brucei* [48,50] suggesting that MitoTam has additional molecular targets besides CI with its NADH dehydrogenase. The EC_{50} value of MitoTam was one or two orders of magnitude higher (but still in in the micromolar range) for other tested organisms such as *Leishmania*, *Acanthamoeba* spp. and the widespread pathogenic yeasts *C. albicans* and *C. neoformans*. MitoTam was the least active against anaerobic protists *Trichomonas vaginalis* and *Giardia intestinalis*, likely due to the absence of conventional energized mitochondria in these organisms [33]. The low activity observed against free-living parasitic amoebae *Naegleria fowleri* requires further research.

Following the encouraging results from *in vitro* testing, we demonstrated that MitoTam significantly decreases parasitemia levels, as well as frequency and size of lesions in animals infected with *T. brucei* and *L. mexicana*, respectively. In agreement with published data [19,22] [23], repeated injection of MitoTam had no apparent adverse effect on BALB/c mice used in our studies.

To investigate the mode of action of MitoTam in unicellular pathogens, we performed comparative proteomic analysis using two distinct model organisms, *T. brucei* (BSF) and *C. albicans*. Only minor changes were detected in the *C. albicans* proteome upon MitoTam treatment, the most upregulated proteins being two homologues of multidrug efflux pumps, possibly explaining the 28 times higher EC_{50} value when compared to BSF *T. brucei* cells. The corresponding analysis in *T. brucei* cells revealed substantial proteome changes upon 12 h MitoTam treatment. Whilst the complexity of the observed alterations failed to pinpoint the exact molecular target(s) of MitoTam, there was a significant impact on the mitochondrion.

To get insight into the complex mode of action that is linked to the function of CI in cancer cells [19], we decided to examine the effect of MitoTam on mitochondrial parameters in BSF *T. brucei*, where the respiratory complex is dispensable [48]. Consistent with studies on cancer and senescent cells [19,22] [23], we found that cells incubated with MitoTam exhibit increased levels of cellular ROS and resulted in rapid dissipation of $\Delta\Psi_m$, which leads to cell death. In contrast, mitochondrial superoxide levels in *T. brucei* cells were decreased upon treatment with MitoTam, indicating that the oxidative burst caused by inhibition of CI-dependent respiration is not responsible for *T. brucei* growth inhibition. Furthermore, *T. brucei* BSF cells incubated with MitoTam exhibited reduced glycerol-3-phosphate-stimulated oxygen consumption, decreased ATP levels, and increased ADP/ATP ratio, suggesting that the biochemical effect of MitoTam could either be due to inhibition of F_oF_1-ATP synthase that generates $\Delta\Psi_m$ in these cells [45,46] or, simply, due to disruption of the mitochondrial membrane integrity, resulting in $\Delta\Psi_m$ collapse.

Our analysis shows that MitoTam at micromolar concentrations significantly increase the membrane permeability of isolated mitochondria, which could be the cause of the altered mitochondrial phenotype. This effect could be due to a direct interaction of the lipophilic MitoTam molecule with the membrane, causing unregulated proton leak, or perhaps due to alteration in membrane fluidity. Disruption of the membrane would indeed rapidly dissipate $\Delta\Psi_m$ in live cells. Alternatively, the effect of MitoTam on membranes may be due to affecting enzymes involved in phospholipid synthesis. Intriguingly, studies on *T. cruzi*, *Leishmania spp*. and *P. falciparum* indicate that tamoxifen, the functional pharmacophore of MitoTam, has an inhibitory effect on phospholipid metabolic pathways [51–53]. Additional experiments are needed to reveal the multifactorial MitoTam mode of action. Nevertheless, our study shows that MitoTam represents a promising candidate to be repurposed as an effective anti-parasitic and anti-fungal compound with high selectivity.

Material and Methods:

340 **Pathogen culture**

341 Culture conditions for all organisms used in this study are summarized in Supplementary Table 4

342

343 **Drug sensitivity assays**

344 The cytotoxicity effect of MitoTam was tested in a variety of organisms. Briefly, cells were seeded in
345 96-well plates at concentrations summarized in Table 4 and grown under standard conditions for 24-
346 120 h, as indicated. The drug was serially diluted in a medium using a two-fold dilution across a plate,
347 resulting in a total volume of 200 µl per well. Each experiment included untreated control cells, as well
348 as a positive control treated with a known growth inhibitory compound for each respective pathogen.
349 The results were statistically analyzed, and dose-response curves plotted using Prism 6.01 (GraphPad
350 Software) and expressed as the half-maximal effective concentration (EC_{50}).

351 The growth of *C. albicans* and *C. neoformans* cultures was determined from OD_{600} values measured on
352 the I-Mark microplate reader (BioRad). *Plasmodium falciparum* dose-response curves were generated
353 using SYBR Green I, as described previously [54]. In brief, triplicate two-fold compound dilution series
354 were set up in 100 µl parasite cultures (~0.2% parasitemia in 2% hematocrit). After two cycles (96 h),
355 parasites were lysed with 20 µl of 6× SYBR green I lysis buffer (0.16% saponin; 20 mM Tris-HCl, 5 mM
356 EDTA, 1.6% Triton X-100, pH 7.4), supplemented with 1:1000 SYBR green I (from 10000× stock, Thermo
357 Fisher). Fluorescence intensity was measured with an Infinite M200 Pro Multimode Microplate Reader
358 (Tecan). *Trypanosoma cruzi* epimastigote cell growth was assessed by CellTiter-Glo 2.0 cell viability
359 assay in a 96-well plate according to the manufacturer's protocol. As indicated, the dose-response
360 curves of *T. brucei* and other pathogens were plotted from cell counts performed on the Guava
361 EasyCyte 8HT flow cytometer (Luminex). The instrument setting and gate selection were adjusted
362 using untreated control for each organism. For *G. intestinalis, A. castellanii,* and *N. fowleri,* that tend
363 to adhere to the walls of the cultivation vessel, were placed on ice for 20 min and subsequently

paraformaldehyde was added to a final concentration of 2% before counting the cells on the flow cytometer.

Trypanosoma brucei growth analysis

T. brucei bloodstream cells were seeded at a concentration of $2x10^5$ and $8x10^5$ cells/ml of 5 ml HMI-9 medium in aerobic culture flasks. Biological triplicates were analyzed including untreated control cultures and cultures treated with final concentrations of 40 nM and 100 nM MitoTam, respectively. Cells were grown under standard growth conditions (37°C, 5% CO_2). At each time point (8, 12, 16, 24, and 48 h), 20 µl were sampled, diluted 10x in fresh HMI-9 and the culture concentration was assessed using Guava EasyCyte 8HT flow cytometer (Luminex). The count parameters and gates were set according to previously measured cultures. In parallel, cells were checked under the microscope at each time point to confirm that live, moving cells were present in each culture.

Trypanosoma brucei dead cell staining

T. brucei BSF cells were seeded at a concentration of $2x10^5$ cells/ml in 5 ml HMI-9 medium in aerobic cultivation flasks. Biological triplicates were set up, including an untreated control group and groups treated with final concentrations of 40 nM and 100 nM MitoTam. The cells were grown under regular growth conditions. At each time point (8, 12, 16, and 24 h), 20 µl were sampled from each flask was sampled, 10x diluted in fresh HMI-9 to a final volume of 200 µl and 2µl of SYTOX Green Dead Cell Stain (Invitrogen) was added to each sample. Cells were incubated at standard growth conditions for 30 min, after which live cell counts were analyzed using Guava EasyCyte 8HT flow cytometer (Luminex). The count parameters and gates were set according to previously measured cultures.

Measurement of ROS production in *T. brucei*

Intracellular and intramitochondrial ROS production was monitored using published protocols [55]. Intracellular ROS levels were evaluated using three biological replicates of approximately $1x10^6$ untreated cells and cells treated with 100 nM MitoTam for 12 h. The samples were collected, incubated with 10 µM of 2',7'-dichlorofluoresceine diacetate (DCFH-DA, Sigma-Aldrich) for 30 minutes and washed with PBS-G (1x PBS with 6 mM glucose). Using a 488 nm excitation laser and a 530/30 nm detector, 10,000 events were immediately counted on the BD FACSCanto II instrument.

Mitochondrial ROS production was assessed using the MitoSOX indicator (Thermo Fisher Scientific) in untreated cells and cells treated with 40 nM or 100 nM MitoTam. An equal number of cells ($1x10^6$) for each treatment was collected, washed in PBS-G, resuspended in HMI-9 medium with 5 µM MitoSOX and stained for 30 min at 37°C, 5% CO_2. After staining, cells were spun down, resuspended in PBS, and immediately analyzed by flow cytometry (BD FACS Canto II Instrument, 488 nm excitation laser and 585/15 nm emission). For each sample, 10 000 events were collected. All values were plotted and statistically analyzed using Prism (8.0) (GraphPad Software).

Comparative label-free proteomics

For *T. brucei* bloodstream forms, a final concentration of 100 nM MitoTam was added to approximately $3x10^7$ cells in the exponential growth phase and cultures incubated for 14 h. Cell viability was checked microscopically before harvesting and washing three times in PBS (1200g, 10 min, 4°C). An untreated control group was prepared in parallel. Both groups were prepared in three biological replicates. The pellets were subjected to reductive alkylation and tryptic digest using routine procedures. Peptides were then analysed by liquid chromatography-tandem mass spectrometry on an ultimate3000 nano rapid separation LC system (Dionex) coupled to an Orbitrap Fusion mass spectrometer (Thermo-Fisher Scientific). Data were analysed as described in [43,56] using label-free quantification in MaxQuant [41] searching the TriTrypDB *T. brucei* strain TREU927 protein database version 54 [57].

For *C. albicans*, approximately 1x10^4 cells were inoculated in RPMI media, as described in [58] and left to grow for 24 h at 35°C without agitation. MitoTam was added to the final concentration of 4.4 µM and cultures incubated for 12 h. Cells were then checked under a microscope, harvested, washed three times with PBS (1 200g, 10 min, 4°C). Pellets were then lyzed using FastPrep 24 5G homogenizer (MP Biomedicals) according to the manufacturer's instructions. Lysates were used for the label-free proteomic analysis and compared with the untreated control group prepared in parallel. Both groups were prepared in three biological replicates. Analysis was performed based on the *C. albicans* protein database downloaded from Uniprot on 12.11.2019 [59]. The threshold settings for comparative proteomic analyses and data processing were chosen as described in [43] for both organisms. Briefly, thresholds were set to Q-value = 0, unique peptides detected >2 and the protein had to be identified at least twice in one of the conditions. For proteins found under only one condition, the average log2 converted intensity of 23 was selected as a minimum threshold. Significantly changed proteins were considered only if the fold change was >2.0.

In the proteomic results of *C. albicans,* localization was predicted based on Uniprot [59]. For *T. brucei* proteomic analysis, manual annotation and localization prediction were based on *T. brucei* 927 database or *T. brucei* bloodstream form mitoproteome database obtained from [44]. Volcano plots were drawn in Perseus 1.6.15.0 [42]. At first, proteins only identified by site, reverse, potential contaminants, and proteins detected in less than two experiments within at least one group were excluded. The imputation was performed using a normal distribution with width 0.3 and downshift of 1.8, separately for each column. The parameters of the volcano plot were set up as following: statistical t-test for both sides, 250 randomizations, false discovery rate of 0.05 and S_0 of 0.1.

Mitochondrial membrane potential measurements

The mitochondrial membrane potential (ΔΨm) of BSF *T. brucei* cells was estimated using the red fluorescent stain MitoTracker Red CMXRos (Invitrogen). MitoTam was added to 5 ml *T. brucei* culture

in an exponential growth phase at a final concentration of 1 µM and cells were incubated for one hour under standard conditions. Subsequently, MitoTracker Red CMXRos was added to a final concentration of 100 nM and samples were incubated for another 10 min. Cultures were spun (1,300 g, 10 min, RT), resuspended in 5 ml of growth medium with 1 µM MitoTam and left for an additional 20 min under standard growth conditions. An untreated control was prepared in parallel. Treated and untreated cells were washed and transferred to 300 µl PBS, spread on microscopy slides, and left to settle. The slides were fixed by immersion in ice-cold methanol for 10 min, once the excess methanol had evaporated, the slides were mounted using Vectashield with DAPI (Vector laboratories), covered with cover slides, and sealed using nail varnish. The slides were imaged on a Leica TCS SP8 WLL SMD-FLIM microscope, using LAS X 3.5.6 imaging software. All images were captured using the exact same microscope setting. Quantification and comparison of signals were performed in NIS-Elements 5.30 (Nikon). Briefly, 10-20 z-stacks were captured using LAS X automatic settings. A single stack with the highest overall intensity was chosen from the batch, and using the Artificial Intelligence module, areas of signal corresponding to individual cells were mapped and the average intensity was determined from the selected area. Furthermore, cell DNA visualized by DAPI was also quantified in the same manner and compared across all images as a reference value. The signal intensity of MitoTracker Red CMXRos was then compared in treated and untreated control, while the intensity of the DAPI signal was used to confirm the reproducibility of the reading.

Estimation of ΔΨm in live cells was performed as described previously [55]. Briefly, an equal number of cells ($1x10^6$) for each treatment was spun (1,400 g, 10 min, RT), the pellets were resuspended in HMI-9 medium with 60 nM TMRE (Thermo Fisher Scientific T669) and stained for 30 min at 37°C, 5% CO_2. After staining, cells were spun down (1,400 g, 10 min, RT) and resuspended in 2 ml of PBS and immediately analyzed by flow cytometry (BD FACS Canto II Instrument). For each sample, 10,000 events were collected. As a control for mitochondrial membrane depolarization, cells were treated with 20 µM protonophore FCCP (carbonyl cyanide 4-(trifluoromethoxy) phenylhydrazone, Sigma).

Data were evaluated using BD FACS Diva software (BD Company) and further analyzed using Prism (8.0) (GraphPad Software).

Estimation of the ΔΨm was also performed using the fluorescent probe Safranine O (Sigma) according to [55]. From each treatment, $2x10^7$ cells were collected, spun down (1,400 g, 10 min, RT), and resuspended in ANT buffer (8 mM KCl, 110 mM potassium gluconate, 10 mM NaCl, 10 mM HEPES, 10 mM K_2HPO_4, 0.015 mM EGTA, 0.5 mg/ml fatty acid-free BSA, 10 mM mannitol, 1.5 mM $MgCl_2$) with 5 µM Safranine O. Intact live cells were permeabilized by the addition of 4 µM digitonin (Calbiochem). The fluorescence of all samples was measured at RT and constant stirring and recorded on a Hitachi F-7100 spectrofluorometer (Hitachi High Technologies) at a 5 Hz acquisition rate, using 495 and 585 nm excitation and emission wavelengths, respectively. As indicated, the reaction was started by adding 1 mM ATP (PanReac AppliChem), F_oF_1-ATP synthase substrate, and stopped by the addition of 10 µg/ml oligomycin (Sigma), F_oF_1-ATP synthase inhibitor. The protonophore SF6847 (Enzo Life Sciences) was added at a final concentration of 250 nM as control for maximal depolarization. Fluorescence data were analyzed using Prism (8.0) (GraphPad Software).

High-resolution respirometry

The effect of MitoTam on respiration was analyzed by Oroboros Oxygraph-2K (Oroboros Instruments Corp., Innsbruck, Austria) as described [55]. Bloodstream form *T. brucei* cells were incubated with 40 nM or 100 nM MitoTam for 16 h and 24 h, as indicated. For each treated sample and control, $2x10^7$ cells were spun down (1,400 g, 10 min, RT) and pellets were washed in Mir05 medium (0.5 mM EGTA, 3 mM $MgCl_2$, 60 mM lactobionic acid, 20 mM taurine, 10 mM KH_2PO_4, 20 mM HEPES, 110 mM sucrose, 1 mg/ml fatty acid-free BSA, pH 7.1). Before the measurement started, the pellets were resuspended in 0.5 ml of Mir05 medium preheated to 37°C and transferred to the respiration chamber. Respiration was monitored at 37°C and with constant stirring. The experiment started with the addition of 10 mM glycerol-3-phosphate (Sigma), the mitochondrial glycerol-3-phosphate dehydrogenase substrate, and

488 respiration was inhibited by the addition of 250 µM SHAM (Salicylhydroxamic acid), the inhibitor of
489 the trypanosomal alternative oxidase. The acquired data were analyzed using Prism (8.0) (GraphPad
490 Software).

491

492 **Western blot analysis**

493 *T. brucei* BSF cells were incubated with 100 nM MitoTam and harvested at different time points after
494 addition as indicated (0h, 8h, 12h, 16h and 24h). Cells were spun down (1,400 g, 10 min, RT), pellets
495 were washed in PBS (pH 7.4) and resuspended in 3xSDS-Page sample buffer (150 mM Tris pH 6.8, 300
496 mM 1,4-dithiothreitol, 6% (w/v) SDS, 30% (w/v) glycerol, 0.02% (w/v) bromophenol blue). The whole-
497 cell lysates were denatured at 97°C for 8 min and stored at -80°C. For Western blot analysis, a volume
498 of sample equal to $2.5x10^6$ cells per well was loaded onto 12% gel, separated by SDS-Page, blotted
499 onto a nitrocellulose membrane (Amersham Protram 0,2 µm PC GE Healthcare Life Sciences) and
500 probed with a monoclonal (mAb) or polyclonal antibody (pAb). Incubation with primary antibodies
501 was followed by a secondary antibody, either HRP-conjugated goat anti-rabbit or an anti-mouse
502 antibody (1:5,000, BioRad). Antibodies were detected using the enhanced chemiluminescence system
503 (Immobilon Forte Western HRP substrate, Merck) on the Amersham Imager 600 (GE Health Care Life
504 Sciences). The PageRuler™ Plus prestained protein ladder (Thermo Fisher Scientific 26619) was used
505 to determine the size of the detected bands. Primary antibodies were: mAb anti-AOX (1:1,000), pAb
506 anti-AAC (1:1,000), anti-VDAC (1:1,000), pAb anti-PYK (pyruvate kinase) 1:1,000 and antibodies against
507 F_oF_1-ATP synthase subunits β (1:2,000), p18 (1:1,000), Tb1 (1:1,000), Tb2 (1:1,000), and OSCP (1:1,000)
508 [55,60].

509

510 **Measurement of the ATP/ADP ratio and total cellular ATP levels**

Changes in the ATP/ADP ratio and total cellular ATP were determined in BSF *T. brucei* cells using the D-luciferin-luciferase bioluminescent enzymatic reaction (assay kit Sigma MAK135) according to manufacturer's instructions. Briefly, from each sample $1x10^6$ cells were harvested and washed once with PBS supplemented with 6 mM glucose (PBS-G). Pellets were resuspended in PBS-G and the mixture transferred into a microtiter plate (96-well white flat-bottom). The bioluminescence signal was recorded in an Orion II microplate luminometer (Titertek Berthold) and analyzed using Prism (8.0) (GraphPad Software).

In situ measurement of ATP levels

Cytosolic and mitochondrial ATP was measured using BSF *T. brucei* cell lines expressing firefly luciferase with or without N-terminal mitochondrial localization signal (MLS) following published protocols [61]. Briefly, MitoTam treated cells, as well as untreated control, were spun ($1x10^7$ cells) (1,400 g, 10 min, RT) and washed in PBS-G. The pellets were resuspended in HEPES-LUC+Glu buffer (10 mM D-glucose, 20 mM HEPES, 116 mM NaCl, 5.6 mM KCL, 8 mM $MgSO_4$, 1.8 mM $CaCl_2$, pH 7.4) and transferred to a 96-well microtiter plate. ATP-dependent luciferase bioluminescence was recorded on a plate reader (Tecan Infinite M100). The light emission was started with the addition of a D-luciferin solution (50 µM; Sigma), collected for 5 min, and statistically analyzed using Prism (8.0) (GraphPad Software).

Determination of the mitochondrial membrane integrity

T. brucei bloodstream mitochondria were isolated by digitonin fractionation, according to [62]. Briefly, approximately $1x10^8$ cells were harvested (1400 g, 10 min, RT) and transferred to Hank's balanced salt solution (Sigma Aldrich). The protein concentrations of the samples were determined by the BCA assay kit (Sigma-Aldrich, USA). Digitonin (Calbiochem) was added to a protein:mass ratio of 1:0.15, lysate

was incubated for 4 min and then spun. The pellet was washed and used as a mitochondria-enriched fraction, while the supernatant was used as a cytosolic fraction. Activities of two marker enzymes were used to assess the purity of fractions and intactness of mitochondrial membranes. The enzyme activities of cytosolic pyruvate kinase (PYK) and mitochondrial threonine dehydrogenase (TDH) were assayed spectrophotometrically at 340 nM by monitoring NADH concentration changes during the reaction. The activity of PYK was measured according to [63] in 0.1M TEA buffer (ThermoFisher Scientific) (final pH 7.6), 5 mM $MgSO_4$ and 50 mM KCl, with the addition of 2.8 mM phosphoenolpyruvate, 2 mM ADP, 0.3 mM NADH and lactate dehydrogenase. The activity of TDH was measured in 0.2M Tris-HCl buffer with 0.25 M KCl (final pH 8.6), with the addition of 120 mM threonine and 2.5 mM NAD^+. Different concentrations of MitoTam were added to the reaction and TDH activity was monitored as a marker for disruption of the mitochondrial membranes. Treatment with nonionic detergent Triton-X100 was used to completely disrupt mitochondrial membranes and thus release maximum TDH activity. Data were statistically analyzed and plotted with Prism (8.0) (GraphPad Software).

Survival analysis in a mouse model

To evaluate the trypanosomiasis effect of MitoTam on the mortality in mice, a group of 14 BALB/c mice was infected IP with approximately $2x10^5$ BSF *T. brucei* cells strain STIB920 and the group of 14 mice was infected with $5x10^5$ BSF cells of *T. brucei brucei* 427 strain, both in 100 µl sterile PBS. Mice were monitored every 12 hours. Based on previous experience with the progression of the disease, half of the infected mice from each group were IV injected with MitoTam (3 mg/kg bw) on days 3 and 5 after infection. The survival of the mice was visually monitored for up to 13 days after infection, the day of death was recorded for each animal.

559 **_T. brucei_ mouse infection model**

560 To assess the effect of MitoTam on the morbidity of trypanosomiasis in mice, sixteen BALB/c mice
561 were infected with $2x10^5$ BSF *T. brucei* cells (strain STIB920) in 100 µl of sterile PBS. On day 2 and 4
562 post infection, eight mice were injected with MitoTam at a final concentration of (3 mg/kg bw).

563 Mice were monitored daily, and blood samples were collected from a tail prick from each animal.
564 Blood drops were smeared on microscopy slides and stained using Wright-Giemsa stain modification,
565 Diff-Quick (Medion Diagnostics) according to the manufacturer's protocol. From each slide three
566 images of random places, where red blood cells were not overlaying, were taken using an inverted
567 widefield microscope Eclipse Ti2 (Nikon) using the CFI Plan Apochromat Lambda 20x objective (Nikon)
568 with NIS-Elements AR 5.20 (Nikon). The images were then processed using the Artificial Intelligence
569 module on NIS-Elements 5.30 (Nikon), manually trained to detect and quantify the number of red
570 blood cells and trypanosomes. The ratio of trypanosomes to red blood cells was calculated and used
571 to plot the data and calculate the statistical difference (student t-test) between the treated and
572 untreated groups in a given days. Data were plotted with Prism (8.0) (GraphPad Software). Animal
573 handling was approved by the Czech Ministry of Agriculture (53659/2019-MZE-18134).

574

575 **_L. mexicana_ mouse subcutaneous leishmaniasis model**

576 The culture conditions of the *L. mexicana* promastigotes were as indicated in Supplementary Table 4,
577 their concentration was determined by hemocytometer. Before infection experiments, promastigotes
578 were harvested, washed three times and resuspended in PBS. Twenty BALB/c mice (ten weeks old)
579 were anesthetized IP with a mixture of ketamine (150 mg/kg) and xylazine (15 mg/kg) and infected
580 intradermally in the ear pinnae by injection of 10^7 promastigotes. For a group of ten animals, MitoTam
581 was administered IP at 1, 2, 3, 5, 6 and 7 weeks after infection at a dose of (3 mg/kg body weight),

other ten animals served as nontreated controls. The presence of lesions was monitored for 12 consecutive weeks.

Rescue assay for *Leishmania spp.* amastigotes

Initially, murine macrophage cells (J774) were seeded in RPMI supplemented with 10% FCS and 50 µg/ml phorbol 12-myristate 13-acetate and left to differentiate for 24 h. Then, after washing the cells once with warm (37°C) serum-free RPMI, stationary phage promastigotes of *L. infantum* or *L. major* were added in a 10:1 ratio ($2.5x10^6$ cell/ml). After 24 h of incubation, cells were washed five times with serum-free RPMI and exposed to increasing concentration of MitoTam (or amphotericin B, as positive control) in RPMI (2% FCS). After two days, macrophages were lysed with 20 µl of 0.05% SDS in RPMI for 30 s and released *Leishmania* cells were incubated with M199 10% FCS for another three days. Finally, the viability of transformed live cells was determined by the resazurin viability assay.

References:

1. Lee SM, Kim MS, Hayat F, Shin D. Recent advances in the discovery of novel antiprotozoal agents. Molecules. 2019;24. doi:10.3390/molecules24213886
2. Monzote L, Siddiq A. Drug Development to Protozoan Diseases. Open Med Chem J. 2011;5: 1–3. doi:10.2174/1874104501105010001
3. Andrews KT, Fisher G, Skinner-Adams TS. Drug repurposing and human parasitic protozoan diseases. Int J Parasitol Drugs Drug Resist. 2014;4: 95–111. doi:10.1016/j.ijpddr.2014.02.002
4. Murphy MP, Smith RAJ. Targeting Antioxidants to Mitochondria by Conjugation to Lipophilic Cations. Annu Rev Pharmacol Toxicol. 2007;47: 629–656. doi:10.1146/annurev.pharmtox.47.120505.105110
5. Teixeira J, Soares P, Benfeito S, Gaspar A, Garrido J, Murphy MP, et al. Rational discovery and

development of a mitochondria-targeted antioxidant based on cinnamic acid scaffold. Free Radic Res. 2012;46. doi:10.3109/10715762.2012.662593

6. Kelso GF, Porteous CM, Coulter C V., Hughes G, Porteous WK, Ledgerwood EC, et al. Selective targeting of a redox-active ubiquinone to mitochondria within cells: Antioxidant and antiapoptotic properties. J Biol Chem. 2001;276: 4588–4596. doi:10.1074/jbc.M009093200

7. Benein P, Almuteri MA, Mehanna AS, D'Souza GGM. Synthesis of triphenylphosphonium phospholipid conjugates for the preparation of mitochondriotropic liposomes. Methods Mol Biol. 2015;1265: 51–57. doi:10.1007/978-1-4939-2288-8_4

8. Du F, Min Y, Zeng F, Yu C, Wu S. A targeted and FRET-based ratiometric fluorescent nanoprobe for imaging mitochondrial hydrogen peroxide in living cells. Small. 2014;10: 964–972. doi:10.1002/smll.201302036

9. Cairns AG, McQuaker SJ, Murphy MP, Hartley RC. Targeting mitochondria with small molecules: The preparation of MitoB and MitoP as exomarkers of mitochondrial hydrogen peroxide. Methods Mol Biol. 2015;1265: 25–50. doi:10.1007/978-1-4939-2288-8_3

10. Terekhova N V., Tatarinov DA, Shaihutdinova ZM, Pashirova TN, Lyubina AP, Voloshina AD, et al. Design and synthesis of amphiphilic 2-hydroxybenzylphosphonium salts with antimicrobial and antitumor dual action. Bioorg Med Chem Lett. 2020;30: 127234. doi:10.1016/j.bmcl.2020.127234

11. Kinnamon KE, Steck EA, Rane DS. A New Chemical Series Active against African Trypanosomes: Benzyltriphenylphosphonium Salts. J Med Chem. 1979;22: 452–455. doi:10.1021/jm00190a019

12. Fueyo González FJ, Ebiloma GU, Izquierdo García C, Bruggeman V, Sánchez Villamañán JM, Donachie A, et al. Conjugates of 2,4-Dihydroxybenzoate and Salicylhydroxamate and Lipocations Display Potent Antiparasite Effects by Efficiently Targeting the Trypanosoma brucei and Trypanosoma congolense Mitochondrion. J Med Chem. 2017;60: 1509–1522. doi:10.1021/acs.jmedchem.6b01740

632 13. Alkhaldi AAM, Martinek J, Panicucci B, Dardonville C, Zíková A, de Koning HP. Trypanocidal
633 action of bisphosphonium salts through a mitochondrial target in bloodstream form
634 Trypanosoma brucei. Int J Parasitol Drugs Drug Resist. 2016;6: 23–34.
635 doi:10.1016/j.ijpddr.2015.12.002
636 14. Long TE, Lu X, Galizzi M, Docampo R, Gut J, Rosenthal PJ. Phosphonium lipocations as
637 antiparasitic agents. Bioorganic Med Chem Lett. 2012;22: 2976–2979.
638 doi:10.1016/j.bmcl.2012.02.045
639 15. Manzano JI, Cueto-Díaz EJ, Olías-Molero AI, Perea A, Herraiz T, Torrado JJ, et al. Discovery and
640 Pharmacological Studies of 4-Hydroxyphenyl-Derived Phosphonium Salts Active in a Mouse
641 Model of Visceral Leishmaniasis. J Med Chem. 2019;62: 10664–10675.
642 doi:10.1021/acs.jmedchem.9b00998
643 16. Taladriz A, Healy A, Flores Pérez EJ, Herrero García V, Ríos Martínez C, Alkhaldi AAM, et al.
644 Synthesis and structure-activity analysis of new phosphonium salts with potent activity against
645 African trypanosomes. J Med Chem. 2012;55: 2606–2622. doi:10.1021/jm2014259
646 17. Jara JA, Castro-Castillo V, Saavedra-Olavarría J, Peredo L, Pavanni M, Jaña F, et al.
647 Antiproliferative and uncoupling effects of delocalized, lipophilic, cationic gallic acid derivatives
648 on cancer cell lines. Validation in vivo in singenic mice. J Med Chem. 2014;57: 2440–2454.
649 doi:10.1021/jm500174v
650 18. Dong L, Gopalan V, Holland O, Neuzil J. Mitocans Revisited: Mitochondrial Targeting as Efficient
651 Anti-Cancer Therapy. Int J Mol Sci. 2020;21: 7941. doi:10.3390/ijms21217941
652 19. Rohlenova K, Sachaphibulkij K, Stursa J, Bezawork-Geleta A, Blecha J, Endaya B, et al. Selective
653 Disruption of Respiratory Supercomplexes as a New Strategy to Suppress Her2 high Breast
654 Cancer. Antioxid Redox Signal. 2017;26: 84–103. doi:10.1089/ars.2016.6677
655 20. Jordan VC. Tamoxifen: a most unlikely pioneering medicine. Nat Rev Drug Discov. 2003;2: 205–
656 213. doi:10.1038/nrd1031
657 21. Unten Y, Murai M, Koshitaka T, Kitao K, Shirai O, Masuya T, et al. Comprehensive understanding

of multiple actions of anticancer drug tamoxifen in isolated mitochondria. Biochim Biophys Acta - Bioenerg. 2022;1863: 148520. doi:10.1016/j.bbabio.2021.148520

22. Hubackova S, Davidova E, Rohlenova K, Stursa J, Werner L, Andera L, et al. Selective elimination of senescent cells by mitochondrial targeting is regulated by ANT2. Cell Death Differ. 2019;26: 276–290. doi:10.1038/s41418-018-0118-3

23. Hubackova S, Zobalova R, Dubisova M, Smigova J, Dvorakova S, Korinkova K, et al. Simultaneous targeting of mitochondrial metabolism and immune checkpoints as a new strategy for renal cancer therapy. Clin Transl Med. Forthcoming 2022.

24. Vacurova E, Trnovska J, Svoboda P, Skop V, Endaya B, Novosadova V, et al. Targeting mitochondria as a novel approach to treatment of metabolic diseases. Nat Commun. Forthcoming 2022.

25. Stuart K, Brun R, Croft S, Fairlamb A, Gürtler RE, McKerrow J, et al. Kinetoplastids: related protozoan pathogens, different diseases. J Clin Invest. 2008;118: 1301–1310. doi:10.1172/JCI33945

26. WHO. Malaria. 2021.

27. Dadar M, Tiwari R, Karthik K, Chakraborty S, Shahali Y, Dhama K. Candida albicans - Biology, molecular characterization, pathogenicity, and advances in diagnosis and control – An update. Microbial Pathogenesis. Academic Press; 2018. pp. 128–138. doi:10.1016/j.micpath.2018.02.028

28. Maziarz EK, Perfect JR. Cryptococcosis. Infectious Disease Clinics of North America. 2016. pp. 179–206. doi:10.1016/j.idc.2015.10.006

29. Grace E, Asbill S, Virga K. Naegleria fowleri: Pathogenesis, diagnosis, and treatment options. Antimicrobial Agents and Chemotherapy. American Society for Microbiology; 2015. pp. 6677–6681. doi:10.1128/AAC.01293-15

30. Kot K, Łanocha-Arendarczyk NA, Kosik-Bogacka DI. Amoebas from the genus Acanthamoeba and their pathogenic properties. Ann Parasitol. 2018;64: 299–308. doi:10.17420/ap6404.164

684 31. Ryan U, Hijjawi N, Feng Y, Xiao L. Giardia: an under-reported foodborne parasite. Int J Parasitol.
685 2019;49: 1–11. doi:10.1016/j.ijpara.2018.07.003
686 32. Van Gerwen OT, Muzny CA. Recent advances in the understanding and management of of
687 Trichomonas vaginalis infection. F1000Research. 2019;8: 1–10.
688 doi:10.12688/f1000research.20411.1
689 33. Tachezy J. Hydrogenosomes and mitosomes mitochondria of anaerobic eukaryotes.
690 Microbiology monographs 9. 2008.
691 34. Field MC, Horn D, Fairlamb AH, Ferguson MAJ, Gray DW, Read KD, et al. Anti-trypanosomatid
692 drug discovery: An ongoing challenge and a continuing need. Nature Reviews Microbiology.
693 Nature Publishing Group; 2017. pp. 217–231. doi:10.1038/nrmicro.2016.193
694 35. Kita K, Nihei C, Tomitsuka E. Parasite Mitochondria as Drug Target: Diversity and Dynamic
695 Changes During the Life Cycle. Curr Med Chem. 2005;10: 2535–2548.
696 doi:10.2174/0929867033456549
697 36. Shingu-Vazquez M, Traven A. Mitochondria and fungal pathogenesis: Drug tolerance,
698 virulence, and potential for antifungal therapy. Eukaryot Cell. 2011;10: 1376–1383.
699 doi:10.1128/EC.05184-11
700 37. Goldberg DE, Zimmerberg J. Hardly Vacuous: The Parasitophorous Vacuolar Membrane of
701 Malaria Parasites. Trends Parasitol. 2020;36: 138–146. doi:10.1016/j.pt.2019.11.006
702 38. De Rycker M, Hallyburton I, Thomas J, Campbell L, Wyllie S, Joshi D, et al. Comparison of a high-
703 throughput high-content intracellular Leishmania donovani assay with an axenic amastigote
704 assay. Antimicrob Agents Chemother. 2013;57. doi:10.1128/AAC.02398-12
705 39. Don R, Ioset JR. Screening strategies to identify new chemical diversity for drug development
706 to treat kinetoplastid infections. Parasitology. 2014;141: 140–146.
707 doi:10.1017/S003118201300142X
708 40. Wyllie S, Brand S, Thomas M, De Rycker M, Chung C wa, Pena I, et al. Preclinical candidate for
709 the treatment of visceral leishmaniasis that acts through proteasome inhibition. Proc Natl Acad

Sci U S A. 2019;116: 9318–9323. doi:10.1073/PNAS.1820175116/SUPPL_FILE/PNAS.1820175116.SAPP.PDF

41. Cox J, Mann M. MaxQuant enables high peptide identification rates, individualized p.p.b.-range mass accuracies and proteome-wide protein quantification. Nat Biotechnol. 2008;26. doi:10.1038/nbt.1511

42. Tyanova S, Temu T, Sinitcyn P, Carlson A, Hein MY, Geiger T, et al. The Perseus computational platform for comprehensive analysis of (prote)omics data. Nat Methods. 2016;13: 731–740. doi:10.1038/nmeth.3901

43. Arbon D, Ženíšková K, Mach J, Grechnikova M, Malych R, Talacko P, et al. Adaptive iron utilization compensates for the lack of an inducible uptake system in Naegleria fowleri and represents a potential target for therapeutic intervention. Singer SM, editor. PLoS Negl Trop Dis. 2020;14: e0007759. doi:10.1371/journal.pntd.0007759

44. Zíková A, Verner Z, Nenarokova A, Michels PAM, Lukeš J. A paradigm shift: The mitoproteomes of procyclic and bloodstream Trypanosoma brucei are comparably complex. PLoS Pathogens. 2017. p. e1006679. doi:10.1371/journal.ppat.1006679

45. Smith TK, Bringaud F, Nolan DP, Figueiredo LM. Metabolic reprogramming during the Trypanosoma brucei life cycle. F1000Research. 2017. doi:10.12688/f1000research.10342.1

46. Schnaufer A, Clark-Walker GD, Steinberg AG, Stuart K. The F1-ATP synthase complex in bloodstream stage trypanosomes has an unusual and essential function. EMBO J. 2005;24: 4029–4040. doi:10.1038/sj.emboj.7600862

47. Nolan DP, Voorheis HP. The mitochondrion in bloodstream forms of Trypanosoma brucei is energized by the electrogenic pumping of protons catalysed by the F1F0-ATPase. Eur J Biochem. 1992;209: 207–216. doi:10.1111/J.1432-1033.1992.TB17278.X

48. Surve S, Heestand M, Panicucci B, Schnaufer A, Parsons M. Enigmatic presence of mitochondrial complex I in Trypanosoma brucei bloodstream forms. Eukaryot Cell. 2011;44: 183–193. doi:10.1128/EC.05282-11

736 49. Gardner MJ, Hall N, Fung E, White O, Berriman M, Hyman RW, et al. Genome sequence of the
737 human malaria parasite Plasmodium falciparum. Nature. 2002;419. doi:10.1038/nature01097
738 50. Verner Z, Čermáková P, Škodová I, Kriegová E, Horváth A, Lukeš J. Complex i (NADH:ubiquinone
739 oxidoreductase) is active in but non-essential for procyclic *Trypanosoma brucei*. Mol Biochem
740 Parasitol. 2011;175: 196–200. doi:10.1016/j.molbiopara.2010.11.003
741 51. Trinconi CT, Miguel DC, Silber AM, Brown C, Mina JGM, Denny PW, et al. Tamoxifen inhibits the
742 biosynthesis of inositolphosphorylceramide in Leishmania. Int J Parasitol Drugs Drug Resist.
743 2018;8: 475–487. doi:10.1016/j.ijpddr.2018.10.007
744 52. Piñero TA, Landoni M, Duschak VG, Katzin AM, Couto AS. Effect of tamoxifen on the
745 sphingolipid biosynthetic pathway in the different intraerythrocytic stages of the apicomplexa
746 Plasmodium falciparum. Biochem Biophys Res Commun. 2018;497.
747 doi:10.1016/j.bbrc.2018.02.183
748 53. Landoni M, Piñero T, Soprano LL, Garcia-Bournissen F, Fichera L, Esteva MI, et al. Tamoxifen
749 acts on Trypanosoma cruzi sphingolipid pathway triggering an apoptotic death process.
750 Biochem Biophys Res Commun. 2019;516: 934–940. doi:10.1016/j.bbrc.2019.06.149
751 54. Johnson JD, Dennull RA, Gerena L, Lopez-Sanchez M, Roncal NE, Waters NC. Assessment and
752 continued validation of the malaria SYBR Green I-based fluorescence assay for use in malaria
753 drug screening. Antimicrob Agents Chemother. 2007;51: 1926–1933. doi:10.1128/AAC.01607-
754 06
755 55. Hierro-Yap C, Šubrtová K, Gahura O, Panicucci B, Dewar C, Chinopoulos C, et al. Bioenergetic
756 consequences of FoF1-ATP synthase/ATPase deficiency in two life cycle stages of Trypanosoma
757 brucei. J Biol Chem. 2021; 100357. doi:10.1016/j.jbc.2021.100357
758 56. Mach J, Bíla J, Ženíšková K, Arbon D, Malych R, Glavanakovová M, et al. Iron economy in
759 Naegleria gruberi reflects its metabolic flexibility. Int J Parasitol. 2018;48: 719–727.
760 doi:10.1016/j.ijpara.2018.03.005
761 57. Aslett M, Aurrecoechea C, Berriman M, Brestelli J, Brunk BP, Carrington M, et al. TriTrypDB: A

functional genomic resource for the Trypanosomatidae. Nucleic Acids Res. 2009;38: 457–462. doi:10.1093/nar/gkp851

58. Clinical and Laboratory Standards Institute (CLSI). Reference Method for Broth Dilution Antifungal Susceptibility Testing of Filamentous Fungi; Approved Standard - CLSI document M38-A2. Clinical and Laboratory Standards Institute (CLSI). 2008. p. 52.

59. Bateman A, Martin MJ, Orchard S, Magrane M, Agivetova R, Ahmad S, et al. UniProt: The universal protein knowledgebase in 2021. Nucleic Acids Res. 2021;49. doi:10.1093/nar/gkaa1100

60. Šubrtová K, Panicucci B, Zíková A. ATPaseTb2, a Unique Membrane-bound FoF1-ATPase Component, Is Essential in Bloodstream and Dyskinetoplastic Trypanosomes. PLoS Pathog. 2015;11. doi:10.1371/journal.ppat.1004660

61. Gnipová A, Šubrtová K, Panicucci B, Horváth A, Lukeš J, Zíková A. The ADP/ATP carrier and its relationship to oxidative phosphorylation in ancestral protist trypanosoma brucei. Eukaryot Cell. 2015;14: 297–310. doi:10.1128/EC.00238-14

62. Šmíd O, Horáková E, Vilímová V, Hrdý I, Cammack R, Horváth A, et al. Knock-downs of iron-sulfur cluster assembly proteins IscS and IscU down-regulate the active mitochondrion of procyclic *Trypanosoma brucei*. J Biol Chem. 2006;281: 28679–86. doi:10.1074/jbc.M513781200

63. Opperdoes FR, Markoš A, Steiger RF. Localization of malate dehydrogenase, adenylate kinase and glycolytic enzymes in glycosomes and the threonine pathway in the mitochondrion of cultured procyclic trypomastigotes of Trypanosoma brucei. Mol Biochem Parasitol. 1981;4: 291–309. doi:10.1016/0166-6851(81)90062-1

Acknowledgment:

The project was supported by the Czech Science Foundation (20-28072S) to RS and 20-14409S to AZ, CePaViP provided by The European Regional Development Fund and Ministry of Education, Youth and Sports of the Czech Republic (reg. no. CZ.02.1.01/0.0/0.0/16_019/0000759) to RS, PV, MZ and AZ, Grant Agency of Charles University (406722) to DA and Fundação para a Ciência e Tecnologia (FCT, Portugal)—PD/BD/128002/2016 for providing funds to MM. We thank to Karel Harant and Pavel Talacko from the Laboratory of Mass Spectrometry, Biocev, Charles University, Faculty of Science, where proteomic and mass spectrometric analysis had been done.

Figure legends:

Figure 1: MitoTam is effective against *T. brucei* and *L. mexicana* parasites *in* mouse infection models.

A) Survival rate of BALB/c mice infected with *T. brucei* was monitored daily for 13 days. Half of the infected mice were injected IV with MitoTam (+MitoTam) on days 3 and 5 (dashed lines) post-infection (3 mg/kg bw). The number of surviving mice from MitoTam treated group (red line) as well as from untreated control group (-MitoTam) (blue line) is plotted against the time (in days).

B) Parasitemia in BALB/c mice infected with *T. brucei* was evaluated microscopically from blood smears. On day 2 and 4 post-infection (dashed lines), eight mice were IV injected with MitoTam (3 mg/kg) (+MitoTam). The ratio of *T. brucei* cells to red blood cells (RBC) was calculated daily and used to quantify the parasitemia levels of each animal from the MitoTam treated group (red line) and the respective untreated control group (-MitoTam) (blue line). Statistically significant differences between the two groups are indicated with an asterisk (unpaired t-test, * $p < 0.05$).

C) Formation of dermal lesions in twenty BALB/c mice was followed for 12 weeks after infection with *L. mexicana*. As indicated (dashed lines), half of the infected animals were injected IP with MitoTam (+MitoTam) at 1, 2, 3, 5, 6 and 7 weeks post-infection. The appearance of lesions was monitored

(+MitoTam, red) and compared to the number of lesions of animals from the untreated control group (-MitoTam, blue).

D) Size of dermal lesions was recorded in ten BALB/c mice infected with *L. mexicana*. Five of the infected animals were treated with MitoTam (+MitoTam) at weeks 2 and 4 post-infection as indicated (dashed lines). Throughout the course of the infection, the lesion areas of each animal were measured weekly. The values were averaged for the MitoTam treated group (+MitoTam, in red) and untreated control group (-MitoTam, in blue). Mean values and error bars representing the standard deviations are shown, statistically significant differences are indicated with an asterisk (paired t-test, *$p < 0.05$).

Figure 2: Global proteome changes upon MitoTam exposure.

Shown are volcano plots of the *t*-test difference from label-free quantification from triplicate experiments, plotted against the respective $-\log_{10}$-transformed *p* values. Untreated control cells were compared to cells treated with MitoTam for *C. albicans* (A) or BSF *T. brucei* (B). **A)** Highlighted points are *C. albicans* significantly upregulated efflux pumps (red dots): P78595 - Multidrug resistance protein CDR2; Q5ANA3 - Pleiotropic ABC efflux transporter of multiple drugs CDR1. **B)** *T. brucei* mitochondrial proteins are in red. **C)** Western blot analyses of whole-cell lysates harvested from BSF *T. brucei* cells treated with 100 nM MitoTam for 0-24 hours as indicated. Equal amounts of total protein were loaded in each lane. A Coomassie stained gel was used as a control for equal loading. The immunoblots were probed with antibodies against cytosolic pyruvate kinase (PYK) and adenine phosphoribosyltransferase (APRT) and mitochondrial heat shock protein 70 (HSP70), proteins associated with the outer mitochondrial membrane (VDAC), inner mitochondrial membrane (AOX, AAC), and subunits of the F_oF_1-ATP synthase (β, p18, OSCP, Tb1, Tb2). The relevant masses of the protein molecular weight are indicated.

Figure 3: MitoTam affects *T. brucei* viability and alters the mitochondrial function of bloodstream *T. brucei* cells.

A) Growth curve of BSF *T. brucei* cultures was evaluated in unstained cells by flow cytometry. Untreated control BSF cells (0 nM MT, blue) were compared with cells incubated with 40 nM MitoTam (40 nM MT, orange) and 100 nM MitoTam (100 nM MT, red). Statistically significant differences are indicated with an asterisk (paired t-test, *p < 0.05, **p < 0.01, ***p < 0.001) (mean ± s.d., n=3).

B) Staining with the cell impermeant nucleic acid dye Sytox was used to distinguish viable (Sytox negative) and dead (Sytox positive) BSF *T. brucei* cells. Concentrations of Sytox negative, live cells are plotted. Untreated control cultures (0 nM MT, blue) were compared with cultures incubated in the presence of 40nM MitoTam (40 nM MT, orange) and 100 nM MitoTam (100 nM MT, red) (paired t-test, *p < 0.05, **p < 0.01, ***p < 0.001) (mean ± s.d., n=3).

Figure 4: Overall effect of MitoTam on the *T. brucei* cell.

A) Production of intracellular ROS in BSF *T. brucei* was quantified by flow cytometry using DCFH-DA detection reagent in untreated control cells (-MT, blue) and cells treated with 100 nM MitoTam for 16 hours (+MT 16 h, red) (mean ± s.d., *n* = 3, **p < 0.01).

B) The O_2 flux per cell using high-resolution respirometry after addition of glycerol-3-phosphate was determined in BSF *T. brucei* untreated control cells (-MT, blue) and BSF cells treated with 100nM MitoTam for 16 hours (+MT 16 h, red) and 24 hours (+MT 24 h, red) (mean ± s.d., *n* = 3, **p < 0.01).

C) Relative ADP/ATP ratio analyzed using a bioluminescence assay kit in BSF *T. brucei* untreated control cells (-MT, blue) and BSF cells treated with 100 nM MitoTam for 16 hours (+MT 16 h, red) and 24 hours (+MT 24 h, red) (mean ± s.d., *n* = 3, ***p < 0.001, ****p < 0.0001).

D) Cytosolic and mitochondrial ATP levels were assessed in transgenic BSF *T. brucei* cell lines expressing firefly luciferase. Untreated control cells (-MT, blue) were compared with cells treated with

100 nM MitoTam for 16 hours (+MT 16 h, red) and 24 hours (+MT 24 h, red). Data were normalized to the values of the untreated control cells and expressed as a percentage (mean ± s.d., *n* = 4).

E) Total cellular ATP levels in BSF *T. brucei* were determined using a bioluminescence assay kit. Data from cultures treated with MitoTam for 16 hours (+MT 16 h, red) and 24 hours (+MT 24 h, red) were normalized to the respective values of the untreated control cells (-MT, blue) and expressed in percentage (mean ± s.d., n = 4), ****p <0.0001).

F) Flow cytometry of TMRE stained cells was used to determine $\Delta\Psi_m$ of BSF *T. brucei*. Data from cultures treated with 100 nM MitoTam for 16 hours (16 h +MT, red) and 24 hours (+MT 24 h, red) were normalized to the respective values of the untreated control cells (-MT, blue) and expressed in percentage. Uncoupler FCCP was added as a control for $\Delta\Psi_m$ depolarization (mean ± s.d., n = 6, ****p<0.0001).

G) *In situ* $\Delta\Psi_m$ was measured in digitonin-permeabilized BSF *T. brucei* cells stained with Safranin O dye. Where indicated, the F_oF_1-ATP synthase substrate – ATP, the F_oF_1-ATP synthase inhibitor - oligomycin (Olgm) and the protonophore SF6847 were added. Representative trace from the measurement of untreated control cells (-MT, blue) in comparison with cells treated with 100nM MitoTam for 16 hours (+MT 16 h, orange) and 24 hours (+MT 24 h, red) is shown.

H) Automated microscopic analysis of BSF *T. brucei* cells stained with Mitotracker Red CMX-ROS was used to determine $\Delta\Psi_m$ in control untreated cells (0 µM MT) and in cells treated with 1 µM of MitoTam for one hour (1 µM MT). Staining with DAPI was used as an internal control for the analysis. Mean signal intensities of Mitotracker Red CMX-ROS and DAPI are depicted on the y-axis (mean ± s.d., ****p<0.0001).

I) *In situ* $\Delta\Psi_m$ was measured in digitonin-permeabilized BSF *T. brucei* cells stained with Safranin O dye. Where indicated, the F_oF_1-ATP synthase substrate – ATP, the F_oF_1-ATP synthase inhibitor - oligomycin (Olgm, green line) and MitoTam (1 µM, red line) were added.

J) Red mitochondrial superoxide indicator MitoSOX was used to detect intramitochondrial ROS production in untreated BSF *T. brucei* control cells (-MT, blue) and BSF cells treated with 100 nM MitoTam for 16 hours (+MT 16 h, red) and 24 hours. Data were normalized to the values of the untreated control cells and expressed as a percentage (+MT 24 h, red) (mean ± s.d., *n* = 6, ****p <0.0001).

K) Integrity of the inner BSF *T. brucei* mitochondrial membrane was assessed in isolated mitochondria incubated with increasing concentration of MitoTam. The mitochondrial enzyme threonine dehydrogenase (TDH) was used as a marker for permeability of the membrane, as the TDH activity is detectable only if a substrate passes freely through compromised mitochondrial membrane (mean ± s.d., *n* = 3).

Supplementary data:

Table S1: Table of screened pathogens summarizing their impact on global health.

Table S2: *C. albicans* proteomic analysis after 12 h of MitoTam exposure.

Proteome comparison of *C. albicans* cultivated in the presence of 4.4 µM MitoTam for 12 h and untreated culture. The table is organized in four sheets: All detected proteins, Downregulated in MitoTam, Upregulated in MitoTam and Raw data. The first three sheets are showing fold-abundance change only for clarity. Upregulated and downregulated proteins were filtered by >2-fold change. Proteins were identified and, where applicable, subcellular localization was annotated based on Uniprot [59].

Table S3: *T. brucei* proteomic analysis after 14h of MitoTam exposure.

903 Proteome comparison of *T. brucei* cultivated in the presence of 100 nM MitoTam for 14 h and
904 untreated culture. Table is organized in four sheets: All detected proteins, Downregulated in MitoTam,
905 Upregulated in MitoTam and Raw data. The first three sheets are simplified to demonstrate fold-
906 abundance change only for clarity. Upregulated and downregulated proteins were filtered by >2-fold
907 change. Where applicable, manual annotation and localization prediction was based on the *T. brucei*
908 927 mitochondrial proteome [44].

909

910 **Table S4: Summary of culture conditions and viability assays for all organisms used in this study.**

911

912 **Figure S1: *Leishmania* sensitivity towards MitoTam evaluated by the intramacrophage assay.**

913 Murine macrophage cell culture J774A.1 was infected with amastigotes of *L. major* (pink line) or *L.*
914 *infantum* (brown line) and incubated with increasing concentration of MitoTam as indicated on the x-
915 axis. Uninfected macrophages (green line) were included as a control.

916

917 **Figure S2: Survival analysis of BALB/c mice infected with *T. brucei.***

918 Survival of infected mice was monitored daily for 8 days. As depicted (dashed lines) half of the infected
919 mice were injected with MitoTam (+MitoTam) on days 2 and 4 post-infection (3 mg/kg body weight).
920 Number of surviving mice from MitoTam treated group (red line) as well as from the untreated control
921 group (-MitoTam) (blue line) are depicted.

922

923 **Figure S3: MitoTam alters the mitochondrial function of bloodstream *T. brucei*.**

924 Cells were incubated with 40 nM of MitoTam for 16 and 24 hours and their mitochondrial parameters
925 were assayed as for 100 nM MitoTam.

A) The O_2 flux per cell using high-resolution respirometry after addition of glycerol-3-phosphate was determined in BSF *T. brucei* untreated control cells (-MT, blue) and BSF cells treated with 40 nM MitoTam for 16 hours (+MT 16 h, red) and 24 hours (+MT 24 h, red) (mean ± s.d., *n* = 3, **p < 0.01, ***p < 0.001).

B) Relative ADP/ATP ratio analyzed using a bioluminescence assay kit in BSF *T. brucei* untreated control cells (-MT, blue) and BSF cells treated with 40 nM MitoTam for 16 hours (+MT 16 h, red) and 24 hours (+MT 24 h, red) (mean ± s.d., *n* = 3).

C) Cytosolic and mitochondrial ATP levels were assessed in transgenic BSF *T. brucei* cell lines expressing firefly luciferase. Results of untreated control cells (-MT, blue) were compared with results of cultures treated with 40 nM MitoTam for 16 hours (+MT 16 h, red) and 24 hours (+MT 24 h, red). Data were normalized to the respective values of the untreated control cells and expressed as a percentage (mean ± s.d., *n* = 4).

D) Total cellular ATP levels in BSF *T. brucei* were determined using a bioluminescence assay kit. Data from cultures treated with MitoTam for 16 hours (+MT 16 h, red) and 24 hours (+MT 24 h, red) were normalized to the values of the untreated control cells (-MT, blue) and expressed in percentage (mean ± s.d., n = 4).

E) Flow cytometry of TMRE stained cells was used to determine $\Delta\Psi_m$ of BSF *T. brucei*. Data from cultures treated with 40 nM MitoTam for 16 hours (16 h +MT, red) and 24 hours (+MT 24 h, red) were normalized to the values of the untreated control cells (-MT, blue) and expressed in percentage. Uncoupler FCCP was added as a control for $\Delta\Psi_m$ depolarization (mean ± s.d., n = 6, ****P <0.0001).

F) *In situ* $\Delta\Psi_m$ was measured in digitonin-permeabilized BSF *T. brucei* cells stained with Safranin O dye. Where indicated, the F_oF_1-ATP synthase substrate – ATP, the F_oF_1-ATP synthase inhibitor - oligomycin (Olgm) and the protonophore SF6847 were added. Representative traces from measurement of

949 untreated control cells (-MT, blue) in comparison with cells treated with 40 nM MitoTam for 16 hours

950 (+MT 16 h, orange) and 24 hours (+MT 24 h, red) are shown.

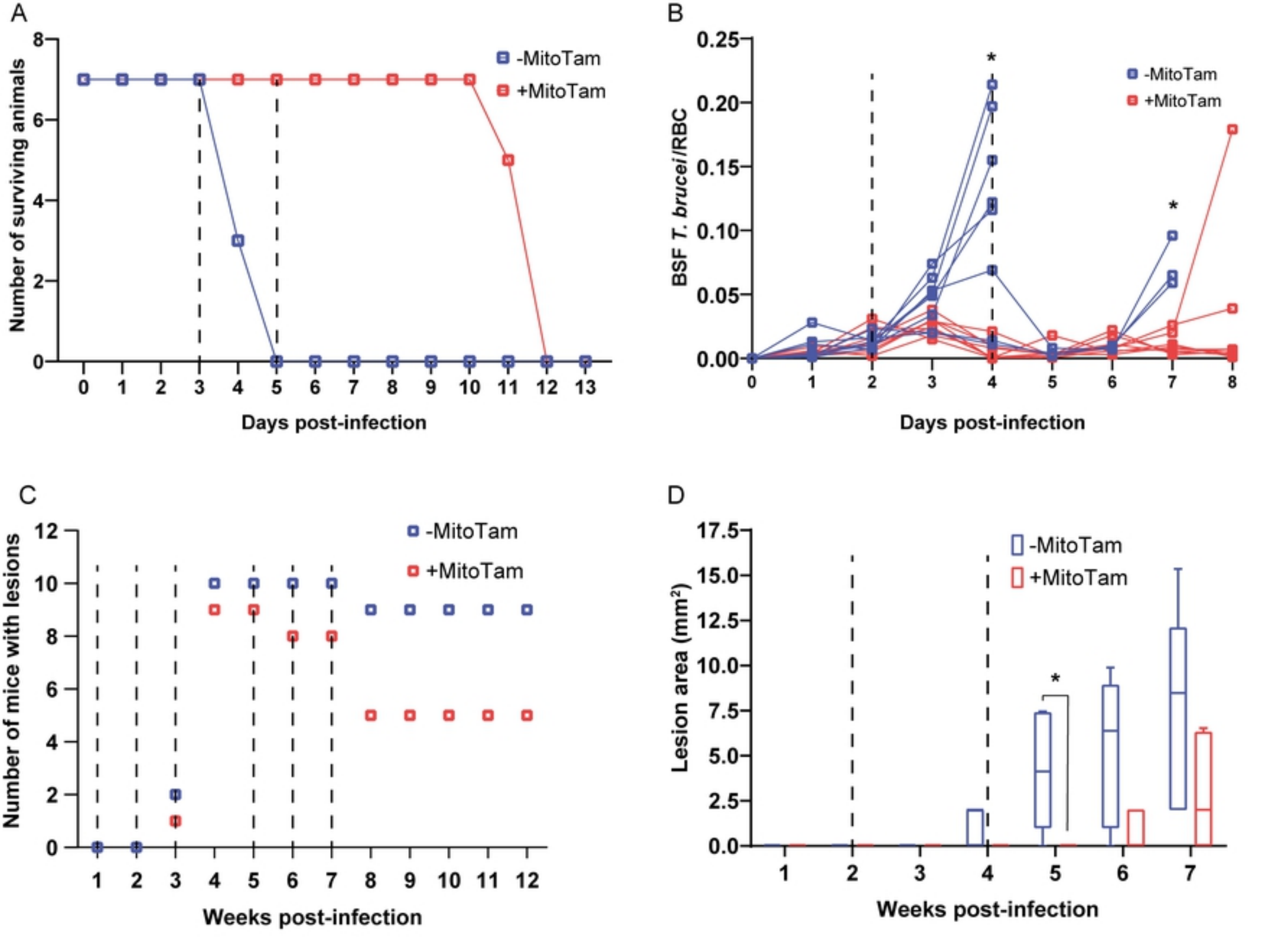
A
Number of surviving animals
-MitoTam
+MitoTam
Days post-infection
B
BSF T. brucei/RBC
-MitoTam
+MitoTam
*
*
Days post-infection
C
Number of mice with lesions
-MitoTam
+MitoTam
Weeks post-infection
D
Lesion area (mm²)
-MitoTam
+MitoTam
*
Weeks post-infection

Fig. 1

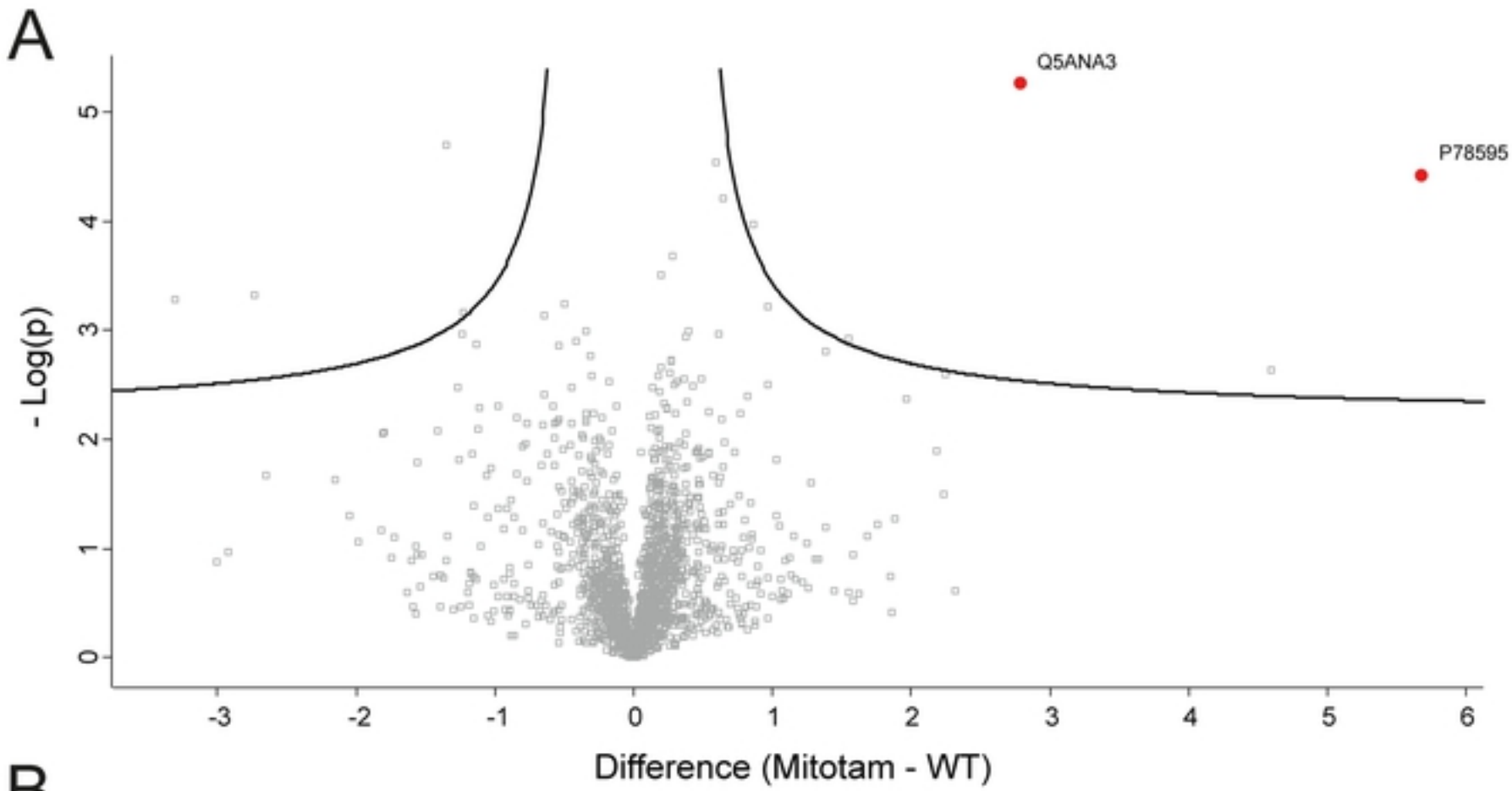

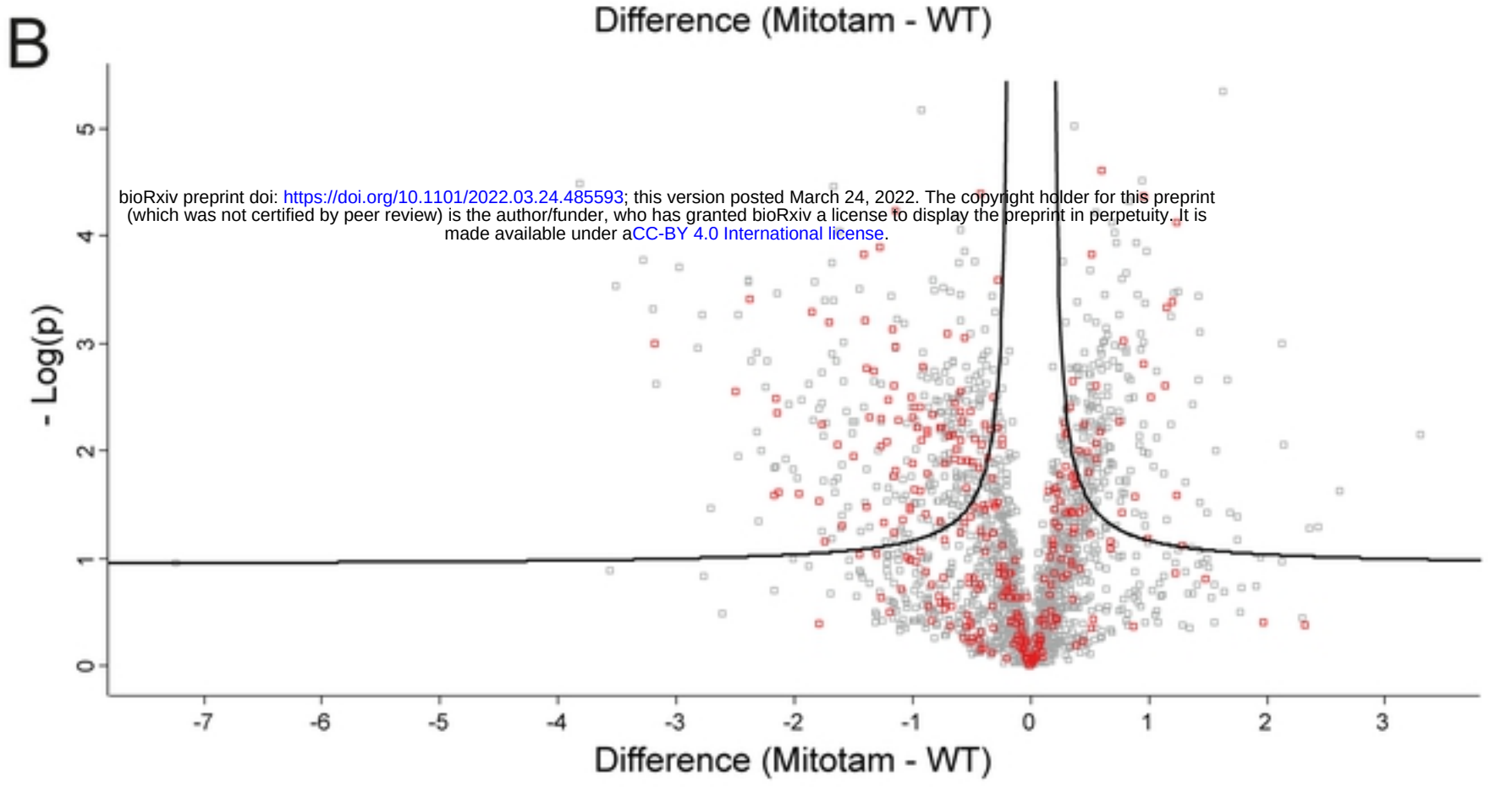

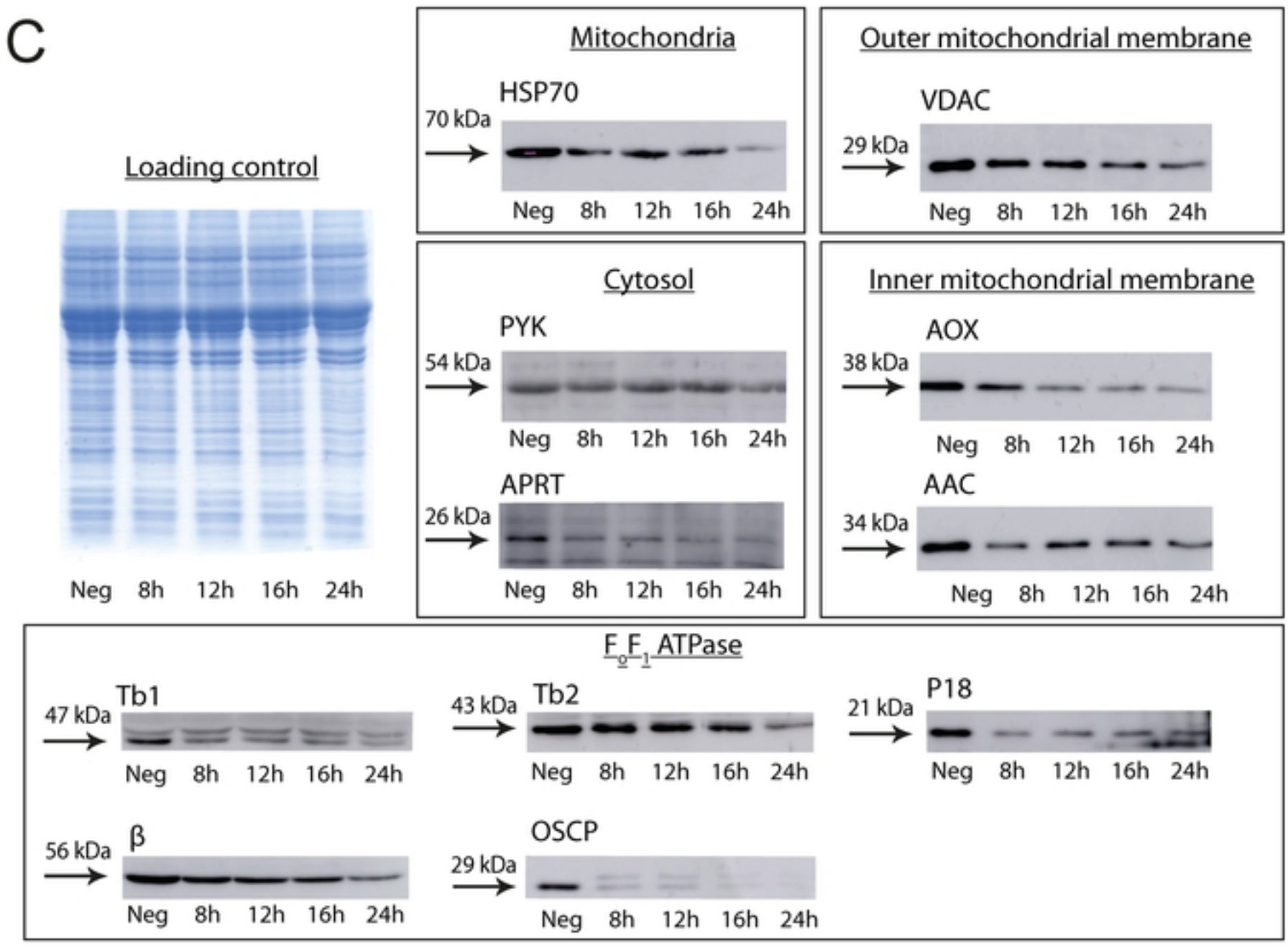

Fig. 2

A

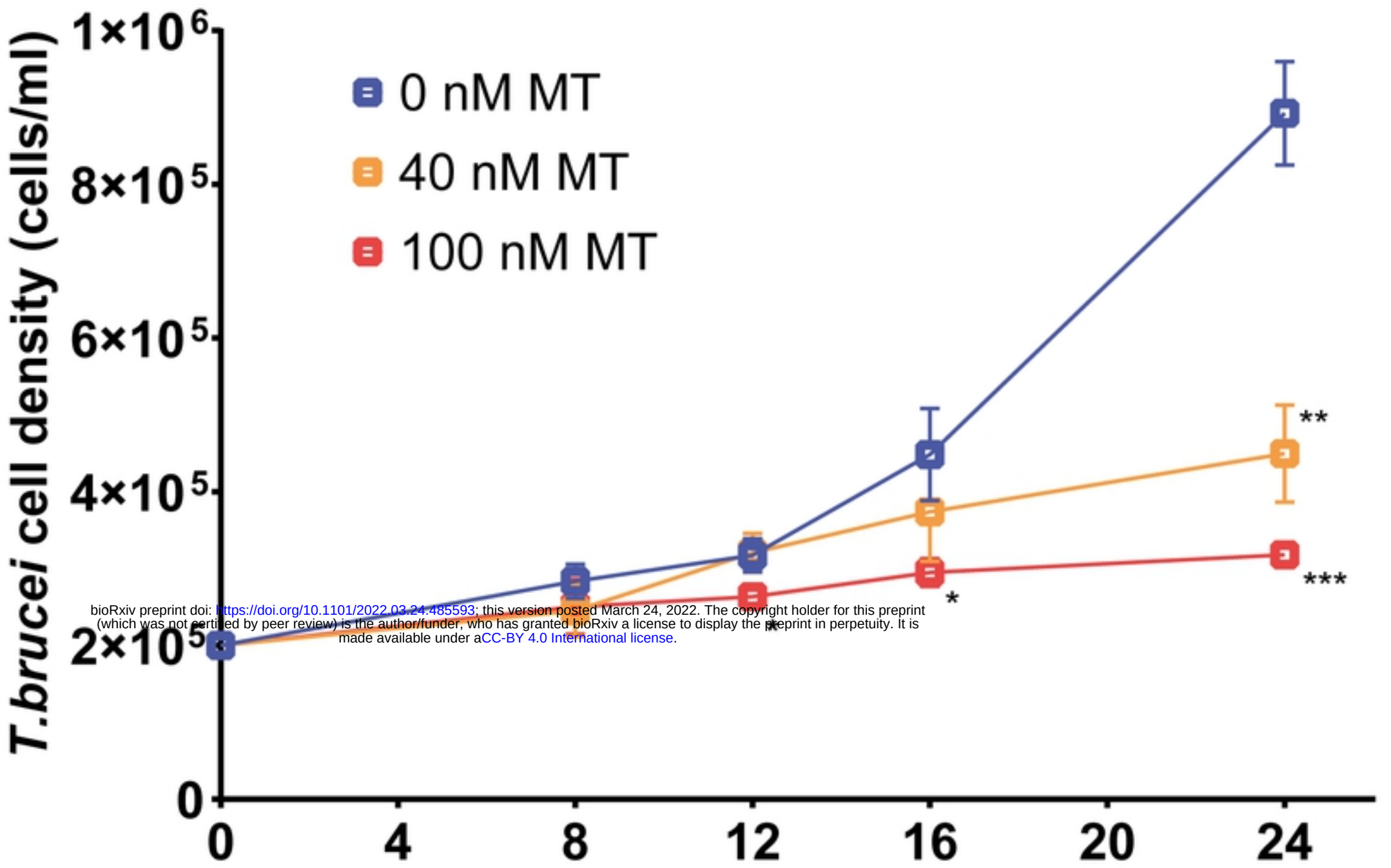

B

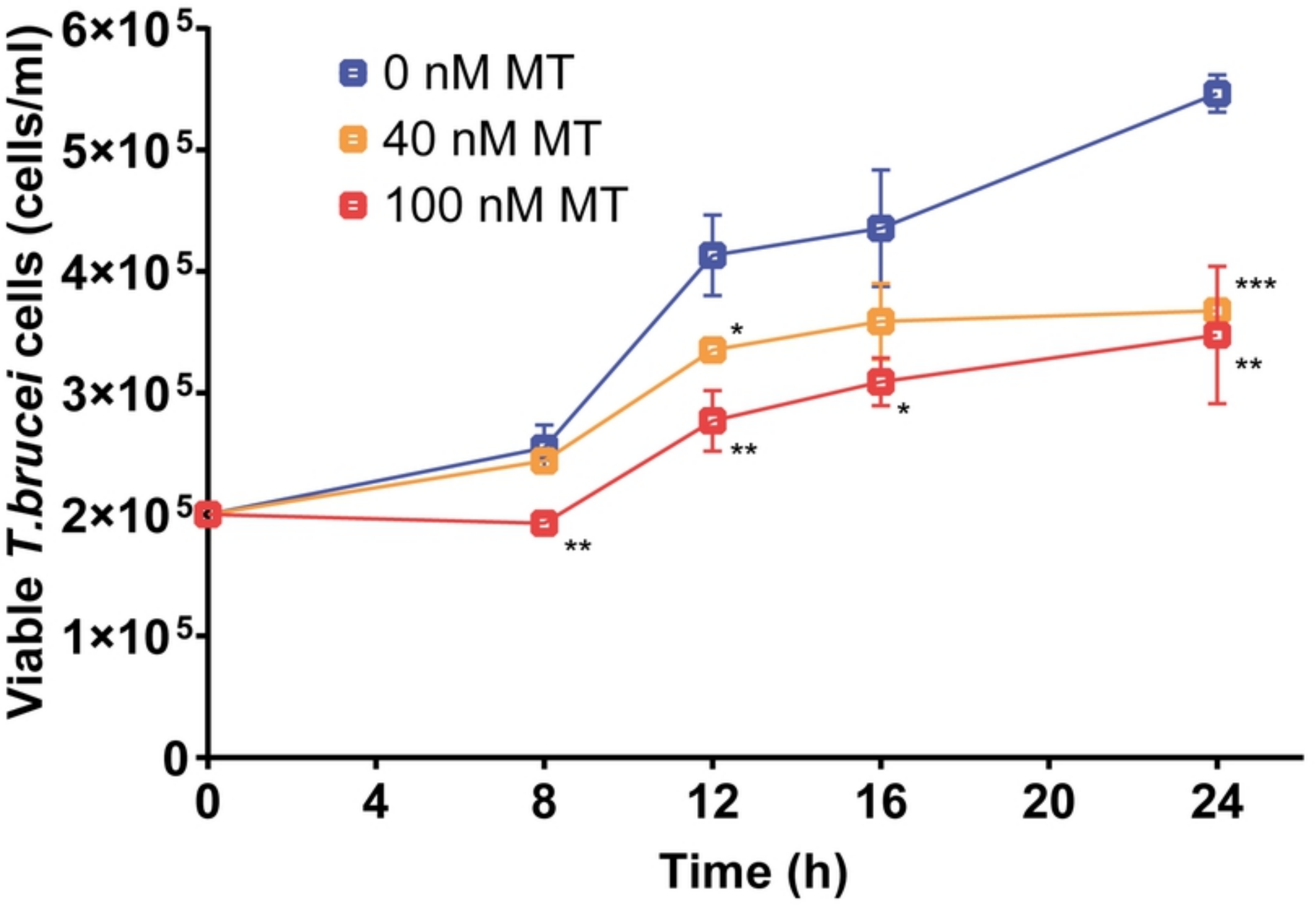

Fig. 3

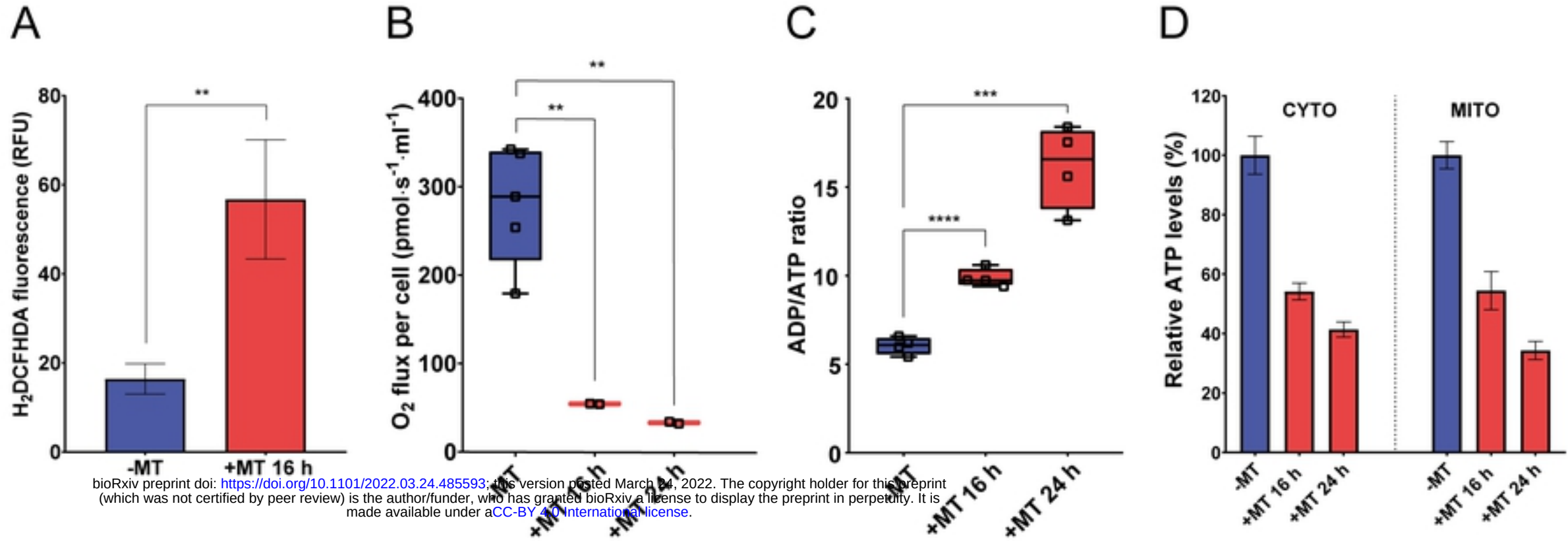

Fig. 4